MMPD: DIVERSE TIME SERIES FORECASTING VIA MULTI-MODE PATCH DIFFUSION LOSS

Anonymous authors
Paper under double-blind review

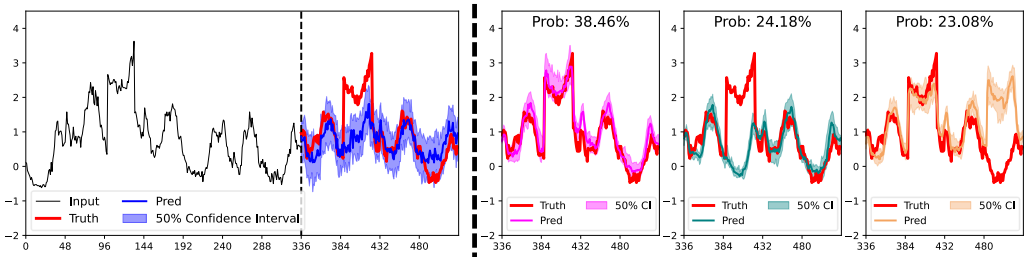

Figure 1: **MSE loss (Left) *vs.* our MMPD loss (Right)** using the same decoder-only Transformer backbone on dataset ETTm1, input 336-predict 192 task. MSE results in a single, ambiguous prediction with a symmetric, constant confidence interval, failing to capture sudden changes in the future. In contrast, our MMPD generates multiple sharp predictions with associated probabilities (only Top-3 predictions are shown), and the confidence intervals are asymmetric and vary over time. More visualizations are shown in Fig. 11 of Appendix J.

ABSTRACT

Despite the flourishing in time series (TS) forecasting backbones, the training mostly relies on regression losses like Mean Square Error (MSE). However, MSE assumes a one-mode Gaussian distribution, which struggles to capture complex patterns, especially for real-world scenarios where multiple diverse outcomes are possible. We propose the Multi-Mode Patch Diffusion (MMPD) loss, which can be applied to any patch-based backbone that outputs latent tokens for the future. Models trained with MMPD loss generate diverse predictions (modes) with the corresponding probabilities. Technically, MMPD loss models the future distribution with a diffusion model conditioned on latent tokens from the backbone. A lightweight Patch Consistent MLP is introduced as the denoising network to ensure consistency across denoised patches. Multi-mode predictions are generated by a multi-mode inference algorithm that fits an evolving variational Gaussian Mixture Model (GMM) during diffusion. Experiments on eight datasets show its superiority in diverse forecasting. Its deterministic and probabilistic capabilities also match the strong competitor losses, MSE and Student-T, respectively.

1 INTRODUCTION

Time series (TS) forecasting have made fast progress. Plenty of backbones have been proposed, incorporating various techniques like sparse attention (Li et al., 2019; Zhou et al., 2021), trend-season decomposition (Wu et al., 2021; Zeng et al., 2023), frequency enhancement (Zhou et al., 2022), patchify (Nie et al., 2023; Zhang & Yan, 2023) and cross-channel dependency (Liu et al., 2023).

Despite the rich works on backbone design, most works rely on regression losses like Mean Square Error (MSE) for training. However, using MSE essentially assumes that the future follows a Gaussian distribution with fixed variance (details in Sec. 3.1). Such a parametric distribution has several limitations, including its symmetric formulation and independent, constant uncertainty.

Most importantly, the single-mode Gaussian cannot support diverse forecasting, where the same past may lead to multiple possible futures. Diverse forecasting is necessary in the real world. On the data side, multi-mode pattern is a fundamental property: identical inputs can diverge into different futures due to unobserved background contexts (Bergmeir, 2024). On the application side, it is a natural requirement in downstream tasks: in domains like trading, an averaged forecast offers little actionable insight, whereas multi-mode predictions enable risk-aware decision (Tsay, 2005).

Therefore, even with carefully designed backbones, the model's capacity remains limited if the training loss cannot capture complex distributions. Several works have attempted to improve loss functions: Le Guen & Thome (2019; 2020) explore the Dynamic Time Warping (DTW). Due to high complexity, DTW-based losses are hard to scale to long-term forecasting. Salinas et al. (2020); Rasul et al. (2023) model the future with negative binomial and Student-T distributions. Woo et al. (2024) uses a mixture of parametric distributions. Although better than MSE, their formulations are still manually predefined, limiting the ability to model complex distributions.

To fill the gap, we propose Multi-Mode Patch Diffusion (MMPD) loss to model complex future distributions. MMPD is generally applicable to any patch-based backbone that divides input series into patches and outputs latent tokens for the future, now one of the most important categories of backbones in both supervised and foundation models. Given one input, models trained with MMPD loss can predict multiple diverse futures (modes), each with an associated probability, as illustrated in the right of Fig. 1. Meanwhile, MMPD loss also integrates with traditional deterministic forecasting, similar to MSE.

Technically, inspired by recent efforts of diffusion on visual tokens (Li et al., 2024a), MMPD constructs a diffusion process for future series conditioned on tokens from upstream forecasting backbones. In Sec. 3.2, we propose a lightweight Patch Consistent MLP as the denoising network in MMPD loss. When denoising a patch, it not only takes the corresponding token as the condition but also considers adjacent noisy patches, ensuring consistency across patches. The integration with deterministic forecasting is achieved by optimizing the diffusion objective at special anchor inputs. As diffusion samples exhibit multi-mode patterns, a multi-mode inference algorithm is devised in Sec. 3.3. It fits an evolving variational Gaussian Mixture Model (GMM) at each diffusion step alongside the reverse process. Priors from the forward process are injected via variational inference to guide the update of GMM. At the end of the reverse diffusion, the GMM outputs multi-mode predictions with corresponding probabilities. **The highlights are:**

1) Beyond the dominant MSE loss that assumes a simple Gaussian distribution, we propose the MMPD loss, leveraging the diffusion process to capture complex distributions. MMPD loss is backbone-agnostic and readily applicable to any patch-based backbone.

2) Observing multi-mode patterns in predictions, we devise a multi-mode inference algorithm that outputs diverse predictions with associated probabilities. Unlike pre-defined mixture distributions (Woo et al., 2024), the number and structure of modes are adaptively inferred, offering greater flexibility.

3) Experiments on eight datasets show the superiority of MMPD loss in diverse forecasting. Its deterministic and probabilistic capabilities also match the best-performing competitor losses, MSE and Student-T, respectively. Its generality is validated on four different backbones.

2 Preliminaries about Diffusion Models

We leave the related works to Appendix A and briefly overview the preliminaries about diffusion models. Given training samples and corresponding conditions (e.g., images and captions): $\mathbf{y}^0, \mathbf{c} \sim q(\mathbf{y}^0, \mathbf{c})$, Diffusion models define a forward Markov process that gradually adds noise to the sample:

$$q(\mathbf{y}^{1:K}|\mathbf{y}^0, \mathbf{c}) = \prod_{k=1}^{K} q(\mathbf{y}^k|\mathbf{y}^{k-1}, \mathbf{c}) \quad q(\mathbf{y}^k|\mathbf{y}^{k-1}, \mathbf{c}) = \mathcal{N}(\mathbf{y}^k; \sqrt{1-\beta_k}\mathbf{y}^{k-1}, \beta_k\mathbf{I}) \tag{1}$$

where $\{\beta_k \in (0,1)\}_{k=1}^K$ is the variance schedule to control the added noise. With the forward process, a reverse Markov process for denoising is modeled by a neural network:

$$p_\phi(\mathbf{y}^{0:K-1}|\mathbf{y}^K, \mathbf{c}) = \prod_{k=1}^{K} p_\phi(\mathbf{y}^{k-1}|\mathbf{y}^k, \mathbf{c}) \quad p_\phi(\mathbf{y}^{k-1}|\mathbf{y}^k, \mathbf{c}) = \mathcal{N}\left(\mathbf{y}^{k-1}; \mu_\phi(\mathbf{y}^k, \mathbf{c}, k), \sigma_k^2\mathbf{I}\right) \tag{2}$$

where σ_k is a step-dependent constant and μ_ϕ represents the neural network that parameterizes the reverse process. The parameters of μ_ϕ are learned by minimizing the negative log-likelihood $\mathbb{E}_{q(\mathbf{x}^0,\mathbf{c})}[-\log p_\phi(\mathbf{x}^0|\mathbf{c})]$. Through parameterization and simplification, the final objective is:

$$\mathcal{L} = \mathbb{E}_{\mathbf{y}^0,\mathbf{c},k,\epsilon}\left[\|\epsilon - \epsilon_\phi(\mathbf{y}^k, \mathbf{c}, k)\|_2^2\right] \quad \mathbf{y}^k = \sqrt{\bar{\alpha}_k}\mathbf{y}^0 + \sqrt{1-\bar{\alpha}_k}\epsilon \quad \epsilon \sim \mathcal{N}(\epsilon; \mathbf{0}, \mathbf{I}) \tag{3}$$

where $\alpha_k = 1 - \beta_k$ and $\bar{\alpha}_k = \prod_{s=1}^{k} \alpha_s$. ϵ_ϕ is a network to parameterize μ_ϕ in Eq. 2. It takes noisy sample $\mathbf{y}^k$, condition $\mathbf{c}$ and diffusion step k as input and outputs the estimated noise in $\mathbf{y}^k$. Once well-trained, new samples can be generated from the reverse process, i.e., Eq. 2.

3 METHODOLOGY

3.1 BROADENING THE DEFINITION OF LOSS FROM A PROBABILISTIC VIEW

Given the past series $\mathbf{x} \in \mathbb{R}^T$, TS forecasting aims to predict values of the same series at the desired future horizon[1] $\mathbf{y} \in \mathbb{R}^\tau$. From a probabilistic view, the task is to model the conditional distribution of the future given its past: $p(\mathbf{y}|\mathbf{x})$. Assuming an independent Gaussian with predicted mean and fixed variance: $p_\theta(\mathbf{y}|\mathbf{x}) = \mathcal{N}(\mathbf{y}; f_\theta(\mathbf{x}), \sigma^2\mathbf{I})$, the objective of maximum likelihood estimation yields:

$$\begin{aligned}\max_\theta \mathbb{E}_{q(\mathbf{x},\mathbf{y})}\left[\log p_\theta(\mathbf{y}|\mathbf{x})\right] &= \max_\theta \mathbb{E}_{q(\mathbf{x},\mathbf{y})}\left[-\frac{1}{2\sigma^2}\left\|\mathbf{y} - f_\theta(\mathbf{x})\right\|_2^2 + \text{Const}\right] \\ &= \min_\theta \mathbb{E}_{q(\mathbf{x},\mathbf{y})}\left[\frac{\tau}{2\sigma^2}\text{MSE}(f_\theta(\mathbf{x}), \mathbf{y})\right]\end{aligned} \tag{4}$$

where $f_\theta(\cdot) : \mathbb{R}^T \to \mathbb{R}^\tau$ is a neural network parameterized by θ to predict the mean. $\sigma \in \mathbb{R}$ is the constant standard deviation. $q(\mathbf{x}, \mathbf{y})$ is the training dataset distribution.

Using gradient-based optimizers like Adam for training, the constant coefficient $\frac{\tau}{2\sigma^2}$ will be absorbed by the step size. Therefore, the following relationship holds (Bishop & Nasrabadi, 2006):

Using MSE loss implicitly assumes the future follows an independent Gaussian distribution, with predicted mean and fixed constant variance.

This assumption is restrictive with limitations: 1) a single-mode Gaussian is unsuitable when multiple distinct futures are possible; 2) predicted steps are assumed independent, yet real-world steps are often correlated; 3) variance is fixed, whereas uncertainty typically evolves over time; 4) the Gaussian is symmetric, but real-world predictions may be asymmetric, e.g., rainfall is nonnegative.

More generally, regardless of how refined the network is, its expressiveness will be limited because MSE assumes a simple, parametric form for the future distribution. The same limitations apply to MAE loss, which assumes a Laplace distribution with predicted location and fixed, independent scale.

To move beyond restricted assumptions and model more complex distributions, we decouple the forecasting network into a ***backbone*** and a ***projector***:

$$f_\theta(\mathbf{x}) = g_\phi(\mathbf{H}), \mathbf{H} = h_\psi(\mathbf{x}), \theta = \{\phi, \psi\} \tag{5}$$

1) The backbone $h_\psi(\cdot)$ extracts latent representations and contains the majority of the parameters. Plenty of backbones with various techniques have been proposed in recent years (Wen et al., 2023).

2) The projector $g_\phi(\cdot)$ maps the representations to the output space, typically via a lightweight MLP with few parameters. Its design highly depends on the chosen distribution—for instance, using a Gaussian with predicted variance requires the projector to output both mean and variance.

Since the backbone is the core and dominates the parameter count, from the perspective of backbone optimization, the projector can be viewed as part of the loss, forming a composite, trainable loss:

$$\min_{\phi,\psi} \text{Loss}^\phi(\mathbf{H}, \mathbf{y}), \mathbf{H} = h_\psi(\mathbf{x}) \tag{6}$$

In this broader definition, the projector g_ϕ acts as an auxiliary module that guides backbone optimization. This is conceptually related to the adversarial loss (Goodfellow et al., 2014), where a learnable discriminator is introduced to guide generator training. Adopting this view, we can design flexible losses that capture richer distributions beyond Gaussian forms. Moreover, traditional losses naturally fall into this framework: MSE can be expressed as: $\text{MSE}^\phi(\mathbf{H}, \mathbf{y}) = \frac{1}{\tau}\left\|\mathbf{y} - g_\phi(\mathbf{H})\right\|_2^2$

3.2 DIFFUSION TRAINING WITH PATCH CONSISTENT MLP

Unlocking the capacity of backbones requires losses corresponding to more flexible distribution families. Leveraging the strong ability to capture complex distributions, we propose a diffusion-based loss, $\text{MMPD}^\phi(\mathbf{H}, \mathbf{y})$. Unlike standalone TS diffusion models relying on specialized architectures (Tashiro et al., 2021), MMPD serves as a plug-and-play loss applicable across various backbones.

In this work, we focus on patch-based backbones, which divide past series into patches as input and output latent tokens for the future[2]. Specifically, in these backbones, past series $\mathbf{x}$ is divided into

[1] We focus on univariate forecasting; for multivariate data, the loss is computed per channel and averaged.

[2] MMPD can also be adapted to non-patch-based backbones with minor modification, as shown in Appendix H

patches of length P and then embedded into T/P latent tokens. Backbones capture dependency among tokens and output latent tokens $\mathbf{H} = \{\mathbf{h}_j\}_{j=1}^{l}, l = \tau/P$, each corresponding to a future patch. As discussed in Appendix A, many recent supervised and pre-training models fall into this category.

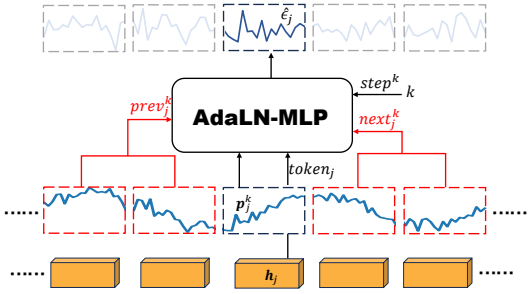

Figure 2: **Patch Consistent MLP** for diffusion. To predict the noise ϵ_j in patch $\mathbf{p}_j^k$, besides the corresponding token $\mathbf{h}_j$ and diffusion step k, adjacent noisy patches centered around j ($\mathbf{p}_{j-r}^k, \ldots, \mathbf{p}_{j-1}^k$ and $\mathbf{p}_{j+1}^k, \ldots, \mathbf{p}_{j+r}^k$ colored in red) are also input to AdaLN-MLP as conditions. This ensures consistency across denoised patches.

The core idea of our MMPD loss is to enable flexible distribution modeling through conditional diffusion, where future latent tokens serve as the condition. To achieve this, a denoising network $\epsilon_\phi(\mathbf{y}^k, \{\mathbf{h}_j\}_{j=1}^{l}, k)$ is required. As an auxiliary module to guide backbone optimization, this denoiser should be lightweight. A straightforward strategy is to split $\mathbf{y}^k$ into patches $\{\mathbf{p}_1^k, \ldots, \mathbf{p}_l^k\}$ and use an MLP to denoise each patch $\mathbf{p}_j^k$ conditioned on token $\mathbf{h}_j$, as done in Li et al. (2024a) for visual tokens. However, such independent MLP models the marginal distribution of each patch $p(\mathbf{p}_j|\mathbf{x}), 1 \le j \le l$ rather than the joint distribution of all future patches $p(\mathbf{p}_1, \ldots, \mathbf{p}_l|\mathbf{x})$. This can lead to inconsistent samples during inference, resulting in discontinuous jumps between patches shown in Fig. 3(a).

To maintain consistency among patches while keeping the denoiser lightweight, we extend Adaptive Layer MLP (AdaLN-MLP) (Peebles & Xie, 2023) to construct the Patch Consistent MLP:

$$
\begin{aligned}
&\epsilon_\phi(\mathbf{y}^k, \{\mathbf{h}_j\}_{j=1}^{l}, k) = [\hat{\epsilon}_1 \bullet \ldots \bullet \hat{\epsilon}_l] \quad \hat{\epsilon}_j = \text{AdaLN-MLP}(\mathbf{p}_j^k, \mathbf{c}_j^k) \\
&\mathbf{c}_j^k = \text{token}_j + \text{step}^k + \text{prev}_j^k + \text{next}_j^k \\
&\text{token}_j = \mathbf{W}^{(token)}\mathbf{h}_j \quad \text{step}^k = \text{Emb}^{(step)}(k) \\
&\text{prev}_j^k = \mathbf{W}^{(prev)}\left[\mathbf{p}_{j-r}^k \bullet \ldots \bullet \mathbf{p}_{j-1}^k\right] \quad \text{next}_j^k = \mathbf{W}^{(next)}\left[\mathbf{p}_{j+1}^k \bullet \ldots \bullet \mathbf{p}_{j+r}^k\right]
\end{aligned}
\tag{7}
$$

As illustrated in Fig. 2, the predicted noise $\hat{\epsilon} \in \mathbb{R}^\tau$ is the concatenation of predicted noise in each patch, i.e., $\hat{\epsilon}_j \in \mathbb{R}^P$. AdaLN-MLP is the denoising MLP from DiT block (Peebles & Xie, 2023), with details in Appendix B. To predict noise in patch $\mathbf{p}_j^k$, the conditioning vector integrates four components: latent tokens token_j, diffusion timestamp step^k, previous and next noisy patches prev_j^k and next_j^k. Here, $\mathbf{W}^{(token)} \in \mathbb{R}^{d_{model} \times d_{model}}$; $\mathbf{W}^{(prev)}, \mathbf{W}^{(prev)} \in \mathbb{R}^{d_{model} \times rP}$ are learnable matrices. $\text{Emb}^{(step)}(\cdot)$ is the positional encoding. r is a constant hyper-parameter that controls the adjacent range around patch j that the MLP can access. Padding is used when $j \le r$ or $j > l - r$.

The key distinction between Patch Consistent MLP and independent MLPs lies in its use of adjacent patches as conditions, i.e., the last line of Eq. 7. Fig. 3(b) shows that this ensures consistency across patches. Moreover, the additional parameters introduced (i.e., $\mathbf{W}^{(prev)}, \mathbf{W}^{(next)}$) are minimal.

Integration with deterministic forecasting. MMPD loss provides a flexible distribution. But in many applications, deterministic forecasting is still needed, which is the role typically served by MSE. A naive solution is to generate multiple samples and take the mean or median. However, diffusion iterations are costly. For efficiency, we integrate deterministic forecasting within the diffusion framework. Considering the diffusion objective (Eq. 3), if the noise cancels the sample at step k^* such that $\mathbf{y}^{k^*} = \mathbf{0}$, the target reduces to a scaled negative ground truth $\epsilon = -\frac{\sqrt{\bar{\alpha}_{k^*}}}{\sqrt{1-\bar{\alpha}_{k^*}}}\mathbf{y}^0$. Thus, we treat $(\mathbf{0}, \{\mathbf{h}_j\}_{j=1}^{l}, k^*)$ as an anchor input for deterministic forecasting and define the joint objective:

$$
\mathcal{L} = \lambda \left\|\epsilon - \epsilon_\phi(\mathbf{y}^k, \{\mathbf{h}_j\}_{j=1}^{l}, k)\right\|_2^2 + (1-\lambda)\left\|\frac{\sqrt{\bar{\alpha}_{k^*}}}{\sqrt{1-\bar{\alpha}_{k^*}}}\mathbf{y}^0 + \epsilon_\phi(\mathbf{0}, \{\mathbf{h}_j\}_{j=1}^{l}, k^*)\right\|_2^2 \tag{8}
$$

where $\lambda = 0.99$ by default balances the probabilistic and deterministic objectives. k^* is set to make $\bar{\alpha}_{k^*}$ close to 0.5 such that $\frac{\sqrt{\bar{\alpha}_{k^*}}}{\sqrt{1-\bar{\alpha}_{k^*}}} \approx 1$. Fig. 9 of Appendix F also shows that prediction accuracy is robust w.r.t k^* across a broad range. After training, the deterministic prediction is directly obtained as $-\frac{\sqrt{1-\bar{\alpha}_{k^*}}}{\sqrt{\bar{\alpha}_{k^*}}}\epsilon_\phi(\mathbf{0}, \{\mathbf{h}_j\}_{j=1}^{l}, k^*)$, bypassing costly diffusion iterations. This integration introduces no new architectures, as it reuses the denoiser ϵ_ϕ. Importantly, the deterministic forecasting term does not conflict with the diffusion term - it is merely a special case of the diffusion objective at the anchor.

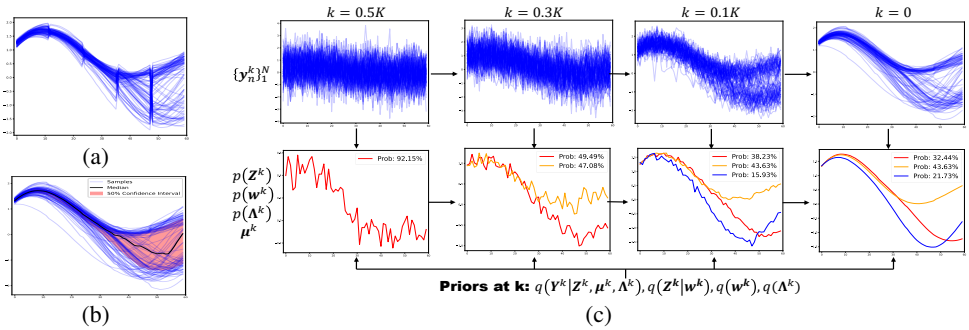

Figure 3: (a) Samples predicted by an independent denoising MLP on dataset Dynamic, showing the inconsistency between patches. (b) Samples predicted by our Patch Consistent MLP, displaying clear multi-mode patterns that are challenging to represent using simple statistics (black line: median, red area: 50% confidence interval). (c) The evolution of our multi-mode inference algorithm: at each step k, posteriors and estimations $p(\mathbf{Z}^k), p(\mathbf{w}^k), p(\mathbf{\Lambda}^k), \boldsymbol{\mu}^k$ are updated via variational EM steps, based on newly generated samples $\{\mathbf{y}_n^k\}_{n=1}^N$. The updates are also guided by priors at each step k.

3.3 Multi-Mode Inference through Evolving Variational GMM

Once trained, we get a flexible distribution $p_\theta(\mathbf{y}|\mathbf{x})$. However, unlike MSE loss that corresponds to a closed-form Gaussian distribution, $p_\theta(\mathbf{y}|\mathbf{x})$ modeled by a diffusion process is an implicit distribution that lacks an explicit analytic form. To summarize this distribution and extract interpretable information for downstream tasks, prior works typically draw samples from it and then compute statistics such as the median and confidence interval (Rasul et al., 2021a; Shen & Kwok, 2023) . However, as shown in Fig. 3(b), the samples exhibit multi-mode patterns, indicating that the same past can lead to multiple possible futures. Such diversity cannot be adequately captured by simple summary statistics.

To address this, we propose a multi-mode inference algorithm that explicitly summarizes distinct outcomes. Suppose the true distribution takes the following multi-mode form:

$$q(\mathbf{y}^0|\mathbf{x}) = \sum_{m=1}^{M} w_m \delta(\mathbf{y}^0 - \mathbf{y}_m^*), \sum_{m=1}^{M} w_m = 1 \tag{9}$$

where $\{\mathbf{y}_m^*\}_{m=1}^M$ denote the M possible predictions and the probability to predict $\mathbf{y}_m^*$ is w_m. To estimate $\{w_m, \mathbf{y}_m^*\}_{m=1}^M$, we combine this multi-mode prior with the forward diffusion process (i.e., Eq. 1), yielding the forward distribution at step k:

$$q(\mathbf{y}^k|\mathbf{x}) = \sum_{m=1}^{M} w_m \mathcal{N}(\mathbf{y}^k; \sqrt{\bar{\alpha}_k}\mathbf{y}_m^*, (1-\bar{\alpha}_k)\mathbf{I}) \tag{10}$$

This is a Gaussian mixture distribution governed by two priors:

1) Mixture weights. The weights w_m remain constant across steps k. In practice, the number of effective modes should be limited, i.e., $w_m \approx 0$ for most modes, to avoid over-fragmented predictions.
2) Covariance matrix. The covariance matrix evolves with k and should be $(1-\bar{\alpha}_k)\mathbf{I}$ at step k.

Consequently, when drawing N samples via reverse diffusion, the collection at step k, $\mathbf{Y}^k = \{\mathbf{y}_n^k\}_{n=1}^N$, should follow the Gaussian mixture distribution in Eq. 10. This observation leads to the use of GMM over other clustering models. By fitting a GMM alongside the reverse process at each step, we can recover $\{w_m, \mathbf{y}_m^*\}_{m=1}^M$ from the final GMM at step 0. To better leverage the priors on mixture weights and covariance, we employ a variational GMM rather than the standard GMM, which enables explicit prior injection. The prior at step k is set as:

$$q(\mathbf{Y}^k|\mathbf{Z}^k, \boldsymbol{\mu}^k, \mathbf{\Lambda}^k) = \prod_{n=1}^{N}\prod_{m=1}^{M} \mathcal{N}(\mathbf{y}_n^k; \boldsymbol{\mu}_m^k, (\Lambda_m^k)^{-1}\mathbf{I})^{z_{nm}^k} \quad q(\mathbf{Z}^k|\mathbf{w}^k) = \prod_{n=1}^{N}\prod_{m=1}^{M} (w_m^k)^{z_{nm}^k}$$
$$\text{\#Prior for mixture weights: } q(\mathbf{w}^k) = \text{Dirichlet}(\mathbf{w}^k; \boldsymbol{\pi}), \pi_m = \rho^{m-1} \tag{11}$$
$$\text{\#Prior for variance: } q(\mathbf{\Lambda}^k) = \prod_{m=1}^{M} \text{Gamma}(\Lambda_m^k; u_m^k, v_m^k), u_m^k = u, v_m^k = u * (1-\bar{\alpha}_k)$$

Algorithm 1 Multi-Mode Inference Algorithm

Input: Future tokens $\{\mathbf{h}_j\}_{j=1}^{l}$, number of samples N to draw via diffusion, maximum number of modes M, prior hyperparameters ρ, u in Eq. 11.
Initialize: Estimation $\{\boldsymbol{\mu}_m^K\}_{m=1}^M$ and parameters in posteriors $\{\widetilde{u}_m^K, \widetilde{v}_m^K, \widetilde{\pi}_m^K\}_{m=1}^M$
Ouput: Statistics and probability of each mode
 # Generate initial samples at step K: $\{\mathbf{y}_n^K\}_{n=1}^N \sim \mathcal{N}(\mathbf{y}^K; \mathbf{0}, \mathbf{I})$
for $k = K-1, \ldots, 0$ **do**
 # Generate samples at step k: $\{\mathbf{y}_n^k\}_{n=1}^N \sim \text{Diffusion}\left(\{\mathbf{y}_n^{k+1}\}_{n=1}^N, \{\mathbf{h}_j\}_{j=1}^l, k+1\right)$
 # E-step: update posterior $p(\mathbf{Z}^k)$
$p(\mathbf{Z}^k) = \prod_{n=1}^{N}\prod_{m=1}^{M}(\widetilde{\gamma}_{nm}^k)^{z_{nm}^k}; \quad \widetilde{\gamma}_{nm}^k = \frac{\gamma_{nm}^k}{\sum_{s=1}^M \gamma_{ns}^k}$
$\ln \gamma_{nm}^k = -\frac{1}{2}\left[\frac{\widetilde{u}_m^{k+1}}{\widetilde{v}_m^{k+1}}\|\mathbf{y}_n^k - \boldsymbol{\mu}_m^{k+1}\|_2^2 + \tau\ln(2\pi)\right] + \frac{\tau}{2}\left[\psi(\widetilde{u}_m^{k+1}) - \ln(\widetilde{v}_m^{k+1})\right] + \psi(\widetilde{\pi}_m^{k+1}) - \psi(\sum_{s=1}^{M}\widetilde{\pi}_s^{k+1})$
 # M-step: update estimation $\boldsymbol{\mu}^k$*, posterior* $p(\mathbf{w}^k), p(\boldsymbol{\Lambda}^k)$
$\boldsymbol{\mu}_m^k = \frac{1}{\widetilde{N}_m^k}\sum_{n=1}^N \widetilde{\gamma}_{nm}^k \mathbf{y}_n^k; \quad \widetilde{N}_m^k = \sum_{n=1}^N \widetilde{\gamma}_{nm}^k$
$p(\mathbf{w}^k) = \text{Dirichlet}(\mathbf{w}^k; \widetilde{\boldsymbol{\pi}}^k); \quad \widetilde{\pi}_m^k = \pi_m + \widetilde{N}_m^k$
$p(\boldsymbol{\Lambda}^k) = \prod_{m=1}^M \text{Gamma}(\Lambda_m^k; \widetilde{u}_m^k, \widetilde{v}_m^k); \widetilde{u}_m^k = u_m^k + \frac{\tau}{2}\widetilde{N}_m^k; \widetilde{v}_m^k = v_m^k + \frac{1}{2}\sum_{n=1}^{N}\widetilde{\gamma}_{nm}^k\|\mathbf{y}_n^k - \boldsymbol{\mu}_m^k\|_2^2$
end for
$\text{Mode}_m = \{\mathbf{y}_n^0 | \arg\max_s \widetilde{\gamma}_{ns}^0 = m\}$
$P(\text{Mode}_m) = |\text{Mode}_m|/N$ and get statistics of each mode

Table 1: Top-3 MSE/MAE, MSE, CRPS evaluations of different losses. The forecasting horizon τ is {96, 192, 336, 720} for the first seven datasets and {60, 120, 180, 300} for Dynamic. Results are averaged over 4 horizons. Rank: average rank on 8 datasets. Bold/underline: best/second. Inf: infinity problem caused by outliers. See Table 7 in Appendix E for full results.

Dataset	ETTh1	ETTm1	ETTh2	ETTm2	WTH	ECL	Traffic	Dynamic	Rank	ETTh1	ETTm1	ETTh2	ETTm2	WTH	ECL	Traffic	Dynamic	Rank
Metric	Top-3 MSE									Top-3 MAE								
MSE	0.430	0.348	0.364	0.264	0.224	0.176	0.433	0.336	3.5	0.440	0.381	0.398	0.320	0.262	0.278	0.326	0.311	4.875
MAE	0.441	0.364	0.368	0.276	0.235	0.179	0.449	0.426	5.25	0.437	0.375	0.392	0.321	0.263	0.272	0.310	0.295	4.125
Gaussian	0.439	0.361	0.379	0.280	0.255	0.165	0.419	0.343	4.75	0.437	0.386	0.411	0.337	0.292	0.256	0.282	0.309	5.125
Student-T	0.430	0.352	0.375	0.286	0.241	0.165	0.416	0.390	4.25	0.428	0.371	0.398	0.333	0.263	0.250	0.261	0.292	3.375
Mix	0.425	0.289	0.343	0.245	0.209	**0.147**	0.412	0.322	1.875	0.426	0.338	0.387	0.308	0.242	0.240	0.261	0.246	2
MMPD	**0.396**	**0.269**	**0.299**	**0.214**	**0.193**	**0.147**	**0.389**	**0.301**	**1**	**0.412**	**0.331**	**0.357**	**0.285**	**0.221**	**0.238**	**0.254**	**0.207**	**1**
Metric	MSE									CRPS								
MSE	0.425	0.350	0.376	0.270	**0.227**	**0.160**	**0.399**	**0.345**	1.875	0.337	0.307	0.308	0.247	0.218	0.270	0.343	0.257	4.25
MAE	0.432	0.355	0.366	0.274	0.233	0.164	0.417	0.426	3.5	0.346	0.313	**0.299**	0.247	0.220	0.288	0.362	0.275	4.625
Gaussian	0.434	0.357	0.382	0.284	0.255	0.163	0.413	0.349	4	0.317	0.282	0.315	0.256	0.228	0.190	0.217	0.233	4.375
Student-T	0.426	0.349	0.372	0.283	0.241	0.164	0.418	0.392	3.5	**0.310**	0.271	0.300	0.250	0.201	**0.187**	0.204	0.224	2.25
Mix	0.446	0.358	0.390	0.285	0.259	0.167	0.426	0.482	6	0.316	**0.269**	0.310	0.247	0.209	Inf	0.205	0.224	3
MMPD	**0.412**	**0.337**	**0.354**	**0.264**	0.229	0.164	0.409	0.353	**1.75**	0.318	0.270	0.301	**0.243**	**0.199**	0.191	**0.202**	**0.203**	**2**

We use $q(\cdot)$ to denote prior distributions and $\{\pi_m, u_m^k, v_m^k\}_{m=1}^M$ without tilde for parameters in priors. $\mathbf{Z}^k = \{\mathbf{z}_n^k\}_{n=1}^N$, where each $\mathbf{z}_n^k$ is a one-hot latent variable indicating the mode $\mathbf{y}_n^k$ belongs to. Line 1 defines the GMM with means $\boldsymbol{\mu}^k = \{\boldsymbol{\mu}_m^k\}_{m=1}^M$, inverse variances $\boldsymbol{\Lambda}^k = \{\Lambda_m^k\}_{m=1}^M$ and mixture weights $\mathbf{w}^k = \{w_m^k\}_{m=1}^M$. Line 2 assigns a constant Dirichlet prior w.r.t diffusion step k for $\mathbf{w}^k$. Its parameter π_m decays by ρ when mode index m increases, encouraging higher-indexed modes to vanish. Line 3 assigns a Gamma prior on $\boldsymbol{\Lambda}^k$ such that $(\mathbb{E}[\Lambda_m^k])^{-1} = v_m^k/u_m^k = 1 - \bar{\alpha}_k$, consistent with the covariance prior. No prior is set for $\boldsymbol{\mu}^k$ as it is related to the unknown $\mathbf{y}_m^*$. The only hyperparameters are ρ and u, with ρ controlling the decay of the Dirichlet prior over mixture weights and u setting the shape of the Gamma prior on variances. Their effects are evaluated in Appenidx F.

With these priors, we get the multi-mode inference Algorithm 1, with detailed derivations in Appendix C. $p(\cdot)$ denote posterior distributions and $\{\widetilde{\pi}_m^k, \widetilde{u}_m^k, \widetilde{v}_m^k\}_{m=1}^M$ with tilde are for parameters in posteriors. As shown in Fig. 3(c), rather than using standard GMM as a post-processing method only applied to $\{\mathbf{y}_n^0\}_{n=1}^N$, we distribute GMM iterations across diffusion steps. This allows us to utilize the knowledge from Eq. 10 via evolving prior distributions, which mitigates the difficulty of GMM initialization and makes a more informed choice of the number of active modes.

4 Experiments

We conduct experiments on: **ETTh1, ETTm1, ETTh2, ETTm2, WTH, ECL, Traffic, Dynamic**. The first seven are widely used datasets from previous works (Nie et al., 2023). The new Dynamic

Table 2: MSE, Mix and MMPD losses over backbones: Crossformer, SegRNN and MaskAE. Horizons are consistent with those in Table 1. #1st: number of first ranks across 8 datasets. Inf: infinity problem caused by outliers. See Table 8&9 in Appendix E for the full results.

Dataset		ETTh1	ETTm1	ETTh2	ETTm2	WTH	ECL	Traffic	Dynamic	#1st	ETTh1	ETTm1	ETTh2	ETTm2	WTH	ECL	Traffic	Dynamic	#1st
Metric		Top-3 MSE									Top-3 MAE								
Crossformer	MSE	0.443	0.378	0.372	0.266	0.223	0.184	0.451	0.331	0	0.452	0.397	0.412	0.323	0.268	0.288	0.342	0.304	0
	Mix	0.433	0.330	0.359	0.236	0.200	0.160	0.424	0.307	0	0.433	0.358	0.400	0.307	0.235	0.255	0.279	0.233	0
	MMPD	**0.381**	**0.310**	**0.315**	**0.228**	**0.197**	**0.152**	**0.404**	**0.295**	**8**	**0.410**	**0.353**	**0.372**	**0.295**	**0.226**	**0.245**	**0.261**	**0.194**	**8**
SegRNN	MSE	0.440	0.385	0.365	0.273	0.222	0.183	0.464	0.333	0	0.451	0.417	0.408	0.337	0.269	0.286	0.333	0.307	0
	Mix	0.435	0.335	0.341	0.248	0.214	0.155	0.439	0.330	0	0.432	0.378	0.389	0.311	0.246	0.245	**0.253**	0.247	1
	MMPD	**0.402**	**0.321**	**0.321**	**0.233**	**0.201**	**0.150**	**0.418**	**0.295**	**8**	**0.426**	**0.375**	**0.377**	**0.305**	**0.234**	**0.242**	0.260	**0.210**	**7**
MaskAE	MSE	0.438	0.354	0.355	0.280	0.226	0.178	0.436	0.339	0	0.447	0.389	0.392	0.337	0.263	0.280	0.329	0.312	0
	Mix	0.415	0.314	0.340	0.253	0.203	0.150	0.416	0.321	0	0.425	0.353	0.384	0.308	0.238	0.241	0.265	0.244	0
	MMPD	**0.399**	**0.280**	**0.311**	**0.247**	**0.197**	**0.144**	**0.387**	**0.296**	**8**	**0.416**	**0.342**	**0.367**	**0.304**	**0.225**	**0.234**	**0.253**	**0.203**	**8**
Metric		MSE									CRPS								
Crossformer	MSE	0.440	**0.382**	0.388	0.271	**0.228**	**0.170**	**0.418**	**0.339**	**5**	0.344	0.316	0.319	0.249	0.221	0.274	0.348	0.253	0
	Mix	0.460	0.399	0.403	0.273	0.241	0.182	0.459	0.455	0	0.323	**0.281**	0.323	**0.248**	**0.202**	Inf	0.217	Inf	3
	MMPD	**0.416**	0.388	**0.374**	**0.270**	0.232	**0.170**	0.420	0.349	4	**0.314**	0.287	**0.316**	0.249	0.204	**0.197**	**0.208**	**0.194**	**5**
SegRNN	MSE	**0.433**	0.383	0.376	**0.279**	**0.226**	0.168	0.428	0.342	**3**	0.341	0.321	0.314	0.259	0.221	0.273	0.345	0.255	0
	Mix	0.452	**0.381**	**0.375**	0.285	0.273	0.187	0.468	0.465	2	Inf	Inf	Inf	Inf	Inf	Inf	Inf	Inf	0
	MMPD	0.434	0.386	0.376	0.285	0.232	**0.167**	**0.421**	**0.341**	**3**	**0.328**	**0.299**	**0.313**	**0.257**	**0.210**	**0.193**	**0.205**	**0.204**	**8**
MaskAE	MSE	0.437	0.357	0.366	0.287	**0.230**	0.162	**0.403**	**0.349**	3	0.341	0.310	**0.303**	0.259	0.220	0.271	0.344	0.259	1
	Mix	0.456	0.371	0.394	0.291	0.270	0.170	0.441	0.476	0	**0.319**	**0.277**	Inf	**0.250**	Inf	0.194	0.208	0.222	3
	MMPD	**0.421**	**0.342**	**0.362**	**0.281**	0.231	**0.161**	0.404	0.350	**5**	**0.319**	**0.277**	0.305	0.258	**0.201**	**0.188**	**0.201**	**0.202**	**6**

consists of 17 signals from a complex dynamical system without obvious periodic patterns. For each dataset, we fix the look-back window T and make predictions on different horizons τ.

Following Top-K accuracy for image classification (He et al., 2016), we use **Top-K MSE/MAE** ($K = 3$ in our setting) to evaluate multi-mode prediction: Top-K modes with the highest probabilities are selected and the minimum MSE/MAE among K modes is reported. Using small K and guided by the probability of each mode, Top-K MSE is more applicable than Best MSE (Le Guen & Thome, 2020), which computes the MSE of all N samples and reports the best. We also report traditional metrics such as **MSE** and **Continuous Ranked Probability Score (CRPS)** to evaluate deterministic and probabilistic accuracy. Detailed setups, including datasets and metrics, are shown in Appendix D.

4.1 Main Results

MMPD *vs.* Baseline Losses. We compare MMPD with the following losses: 1) deterministic losses **MSE** (Nie et al., 2023) and **MAE** (Liu et al., 2022a); 2) distribution-based losses **Gaussian** (Salinas et al., 2020) and **Student-T** (Rasul et al., 2023); 3)**Mix** (Woo et al., 2024) that mixes multiple parametric distributions for flexible modeling. We maintain the main backbone as a patch-based decoder-only Transformer (Goswami et al., 2024; Lin et al., 2024b) and change the losses.

Top-3 MSE and Top-3 MAE in Table 1 show that only Mix and MMPD can capture multi-mode patterns. Among them, our MMPD loss consistently outperforms Mix, as the number and form of mixture components in Mix are predefined, while in MMPD, they are learned directly from the data. Regarding deterministic forecasting performance measured by MSE, our MMPD loss is comparable to the best competitor, MSE loss, and even outperforms it on some datasets, showing MMPD effectively integrates deterministic forecasting. Similarly, MMPD performs on par with the best-performing baseline, Student-T, in terms of probabilistic forecasting measured by CRPS.

Generality of MMPD Loss across Backbones. Besides the decoder-only Transformer used in Table 1, we also compare MMPD loss with MSE and Mix across the following three backbones: 1) channel-mixing Transformer **Crossformer** (Zhang & Yan, 2023), 2) patch-based RNN **SegRNN** (Lin et al., 2023), 3) Masked AutoEncoder using pure Transformers **MaskAE** (Zhang et al., 2024b). Results in Table 2 demonstrate that the diverse forecasting capability of MMPD significantly outperforms MSE and Mix across all three backbones. The deterministic forecasting ability measured by MSE is comparable to MSE loss, which is consistent with Table 1. It is worth noting that, due to the log-normal component, Mix loss is likely to generate outliers, leading to the infinity problem in CRPS. This issue is particularly severe for the RNN-based SegRNN. In contrast, the CRPS of the MMPD loss remains stable, regardless of whether the upstream backbone is an RNN or a Transformer.

4.2 Model Analysis

Ablation of Patch Consistent MLP. In Fig. 4(a), the independent MLP, which does not incorporate adjacent patches ($r = 0$), performs poorly in multi-mode prediction, with the Top-3 MSE even exceeding MSE. This occurs because the independent MLP only models the marginal distribution of each patch $p_\theta(\mathbf{p}_j|\mathbf{x})$ rather than the joint distribution of all patches, leading to inconsistent samples as shown in Fig. 3(a). In contrast, the Patch Consistent MLP, even with $r = 1$, significantly reduces both Top-3 MSE and Top-3 MAE. Further increasing r slightly improves performance.

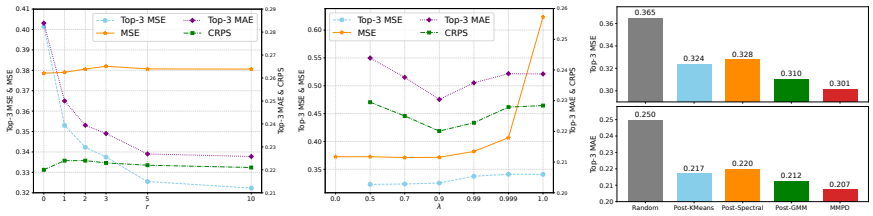

(a) (b) (c)

Figure 4: (a) Metrics for varying adjacent range r in Patch Consistent MLP ($r = 0$: independent MLP) on Dynamic (prediction horizon $\tau = 180$). (b) Metrics for varying probabilistic/deterministic objective balancing weight λ, with all other settings identical to (a). (c) Top-3 MSE/MAE comparison between multi-mode inference and post-processing methods.

Effect of Balancing Weight λ in Eq. 8. Fig. 4(b) shows that when training with only the diffusion objective ($\lambda = 1.0$), the deterministic prediction capability measured by MSE is poor. Decreasing it to 0.999, the MSE is greatly reduced, while other metrics are not harmed. As λ gradually decreases, MSE improves and stabilizes. An interesting observation is that when λ decreases from 1.0 to 0.9, besides MSE, other multi-mode and probabilistic metrics also get better. We suspect that this is the collaborative effect brought by joint training of the two objectives.

Ablation of Multi-Mode Inference Algorithm. Fig. 4(c) compares our multi-mode inference algorithm with various post-processing methods. Random assignment performs the worst, highlighting the necessity of multi-mode extraction. Our multi-mode inference algorithm significantly outperforms KMeans and spectral clustering. Furthermore, MMPD surpasses Post-GMM, which uses the same GMM formulation as MMPD but is applied directly to final samples $\{\mathbf{y}_n^0\}_{n=1}^N$ without the evolving priors. This stems from fitting an evolving GMM with dynamic priors on gradually denoised samples, which mitigates the difficulty of parameter initialization in GMM and automatically selects a more appropriate number of activated modes. Due to page limit, other hyperparameter evaluations (e.g., noise schedule, diffusion steps, hyperparameters in Algorithm 1) are provided in Appendix F.

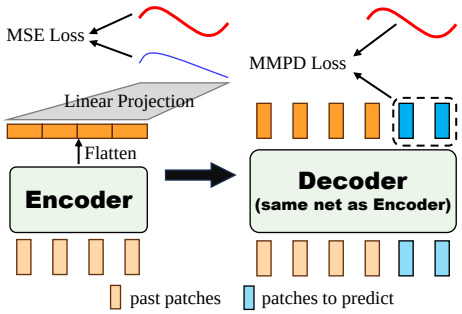

Figure 5: Approach for adapting encoder-only backbones to use MMPD loss: learnable tokens, indicating the patches to predict, are appended to the end of the past patch sequence. The padded sequence is fed to the same network as encoder, transforming the backbone into a decoder-only model. Only the output tokens corresponding to the future series are used for MMPD loss computation.

Adapting Encoder-Only Backbones for MMPD Loss. In the left of Fig. 5, besides backbones we have evaluated, there are encoder-only backbones that flatten the encoder outputs and linearly project them to predict the series for MSE loss (Nie et al., 2023; Luo & Wang, 2024). They do not generate future latent tokens, meaning MMPD loss cannot be directly applied. In the right of Fig. 5, we transform them into decoder-only ones for our MMPD loss by appending learnable tokens to the end of the input sequence.

We adapt the encoder-only PatchTST (Nie et al., 2023) into a decoder-only backbone to enable MMPD. In Fig. 6(a)&6(c), the scale of the projection layer in encoder-only version increases with input/output lengths, while remaining constant with our adaptation. Decoder-only PatchTST with MMPD gets lower MSE, indicating better scalability. Also, our adaptation enables multi-mode and probabilistic forecasting, evidenced by improved Top-3 MSE and CRPS in Fig. 6(b)&6(d).

MMPD Loss *vs.* Standalone TS Diffusion Models. We also compare MMPD loss with standalone TS diffusion models **1)CSDI** (Tashiro et al., 2021), **2)TSDiff** (Kollovieh et al., 2023), **3)MG-TSD** (Fan et al., 2024), **4)Diffusion-TS** (Yuan & Qiao, 2024). These models involve complex denoising networks, making long-term experiments conducted in Sec. 4.1 challenging. Following Tashiro et al. (2021), we forecast the next 24 steps using the past 96 on ETTh1. Results in Table 3 show that our MMPD significantly outperforms standalone diffusion models. This is because the decoupling from the backbone allows the MMPD loss to fully leverage the advanced backbone. Moreover, the lightweight denoising MLP in MMPD ensures faster inference compared to diffusion models with heavier networks and complex diffusion processes.

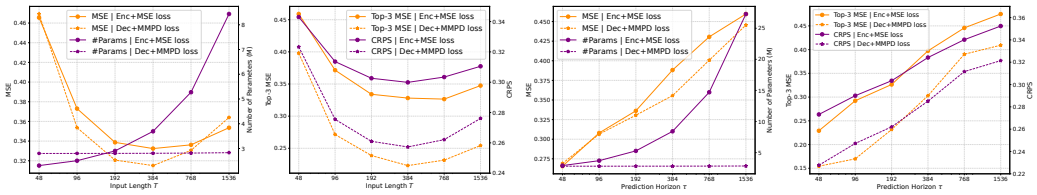

(a) (b) (c) (d)

Figure 6: Comparison of adapted decoder-only PatchTST (Nie et al., 2023) with MMPD loss (Dec+MMPD loss) against the original encoder-only version with MSE loss (Enc+MSE loss). (a), (b): number of parameters and metrics (MSE, Top-3 MSE and CRPS) for varying input length T on ETTm1, the prediction horizon is set to $\tau = 192$. (c), (d): number of parameters and metrics for varying prediction horizon τ on ETTm1, the input length is set to $T = 768$.

Table 4: FLOPs across structures/stages for MSE Loss, TS Diffusion Models and MMPD Loss. S: number of blocks in MLPs, d (short for d_{model}): hidden state dimension. $F_{bkb}, F_{MLP}, F_{PC-MLP}$: FLOPs of backbone, conventional MLP and Patch Consistent MLP. GMM FLOPs in MMPD are omitted as they are negligible vs. neural networks. See derivation in Appendix G.

Structure/Stage	MSE Loss	TS Diffusion Models	MMPD Loss
MLP Projector	$F_{MLP} = O(\frac{\tau}{P}[(2S+1)d^2 + Pd])$	N/A	$F_{PC-MLP} = O(\frac{\tau}{P}[(5S+3)d^2 + (2r+2)Pd])$
Training (forward only)	$F_{bkb} + F_{MLP}$	F_{bkb}	$F_{bkb} + 2F_{PC-MLP}$
Deterministic Inference	$F_{bkb} + F_{MLP}$	N/A	$F_{bkb} + F_{PC-MLP}$
Prob/Multi-Mode Inference	N/A	NKF_{bkb}	$F_{bkb} + NKF_{PC-MLP}$

Table 5: Memory, training (per batch) and inference time (per instance) of MSE Loss, Diffusion-TS and MMPD Loss on dataset WTH, $T = 336, \tau = 192$, batch $= 32, N = 100, K = 20$.

Stage	MSE Loss		Diffusion-TS		MMPD Loss	
	Memory (GB)	Time (ms)	Memory (GB)	Time (ms)	Memory (GB)	Time (ms)
Training	2.599	89.9	4.358	676.4	2.930	106.3
Deterministic Infer	0.031	2.3	N/A		0.034	3.1
Prob/Multi-Mode Infer	N/A		11.245	28,495.1	0.505	415.8

Table 3: Evaluation of MMPD loss against TS diffusion models on ETTh1, $T = 96, \tau = 24$. "Time" refers to average inference time per instance.

	Top-3 MSE	Top-3 MAE	MSE	CRPS	Time(s)
CSDI	0.225	0.304	0.339	0.265	1.014
TSDiff	0.275	0.336	0.345	0.292	0.419
MG-TSD	0.287	0.331	0.340	0.306	0.217
Diffusion-TS	0.282	0.324	0.351	0.294	0.520
Decoder+MMPD	**0.186**	**0.280**	**0.298**	**0.254**	**0.075**

Efficiency Analysis. As shown in Table 4, the Patch Consistent MLP for MMPD incurs marginally higher FLOPs than the conventional MLP for MSE loss. During training, MSE loss requires one MLP forward pass, while MMPD loss requires two: one for the diffusion objective and another for the deterministic in Eq. 8. However, since the backbone dominates training cost (i.e., $F_{bkb} >> F_{MLP}, F_{PC-MLP}$), the total training FLOPs of MMPD remain nearly identical to those of MSE. This equivalence also holds for deterministic inference, where both losses require a single MLP pass. For probabilistic and multi-mode inference, which MSE cannot perform, MMPD's overhead is significantly lower than that of standalone TS Diffusion models, as MMPD only requires a single heavy backbone pass followed by multiple lightweight MLP passes. The theoretical analysis is consistently supported by the experimental memory occupancy and speed measurements in Table 5.

5 Further Discussions and Conclusion

In Appendix H, we extend MMPD beyond its basic setting to non-patch-based backbones by inserting a Transformer decoder layer between the backbone and MMPD loss. In Appendix I, beyond the single-dataset paradigm, we further apply MMPD to a multi-task model, UNITS (Gao et al., 2024), to perform multi-task, few-shot and zero-shot forecasting. In both cases, MMPD functions as a plug-and-play loss that can be incorporated with minimal changes. Compared with original models trained with MSE loss, MMPD preserves deterministic forecasting performance while enabling richer distribution modeling, supporting multi-mode and probabilistic forecasting.

In conclusion, we have proposed MMPD, a diffusion-based loss that goes beyond the dominant single-mode MSE loss in TS forecasting. By modeling complex distributions, MMPD equips models with multi-mode forecasting capabilities—an essential feature for many real-world applications, particularly those involving risk-aware decision making. Extensive benchmark experiments demonstrate the effectiveness and broad applicability of our approach.

REFERENCES

Juan Miguel Lopez Alcaraz and Nils Strodthoff. Diffusion-based time series imputation and forecasting with structured state space models. *Transactions on Machine Learning Research (TMLR)*, 2022.

Christoph Bergmeir. Fundamental limitations of foundational forecasting models: The need for multimodality and rigorous evaluation. In *Workshop at NeurIPS*, 2024.

Christopher M Bishop and Nasser M Nasrabadi. *Pattern recognition and machine learning*. 2006.

Si-An Chen, Chun-Liang Li, Sercan O Arik, Nathanael Christian Yoder, and Tomas Pfister. Tsmixer: An all-mlp architecture for time series forecasting. *Transactions on Machine Learning Research (TMLR)*, 2023.

Marco Cuturi and Mathieu Blondel. Soft-dtw: a differentiable loss function for time-series. In *International Conference on Machine Learning (ICML)*, 2017.

Xinyao Fan, Yueying Wu, Chang Xu, Yuhao Huang, Weiqing Liu, and Jiang Bian. Mg-tsd: Multi-granularity time series diffusion models with guided learning process. In *International Conference on Learning Representations (ICLR)*, 2024.

Valentin Flunkert, David Salinas, and Jan Gasthaus. Deepar: Probabilistic forecasting with autoregressive recurrent networks. *International Journal of Forecasting*, 2017.

Shanghua Gao, Teddy Koker, Owen Queen, Tom Hartvigsen, Theodoros Tsiligkaridis, and Marinka Zitnik. Units: A unified multi-task time series model. In *Conference on Neural Information Processing Systems (NeurIPS)*, 2024.

Tilmann Gneiting and Adrian E Raftery. Strictly proper scoring rules, prediction, and estimation. *Journal of the American statistical Association*, 2007.

Ian J Goodfellow, Jean Pouget-Abadie, Mehdi Mirza, Bing Xu, David Warde-Farley, Sherjil Ozair, Aaron Courville, and Yoshua Bengio. Generative adversarial nets. In *Conference on Neural Information Processing Systems (NeurIPS)*, 2014.

Mononito Goswami, Konrad Szafer, Arjun Choudhry, Yifu Cai, Shuo Li, and Artur Dubrawski. Moment: A family of open time-series foundation models. In *International Conference on Machine Learning (ICML)*, 2024.

Kaiming He, Xiangyu Zhang, Shaoqing Ren, and Jian Sun. Deep residual learning for image recognition. In *IEEE / CVF Computer Vision and Pattern Recognition Conference (CVPR)*, 2016.

Jonathan Ho, Ajay Jain, and Pieter Abbeel. Denoising diffusion probabilistic models. In *Conference on Neural Information Processing Systems (NeurIPS)*, 2020.

Qihe Huang, Lei Shen, Ruixin Zhang, Shouhong Ding, Binwu Wang, Zhengyang Zhou, and Yang Wang. Crossgnn: Confronting noisy multivariate time series via cross interaction refinement. In *Conference on Neural Information Processing Systems (NeurIPS)*, 2023.

Ming Jin, Shiyu Wang, Lintao Ma, Zhixuan Chu, James Y Zhang, Xiaoming Shi, Pin-Yu Chen, Yuxuan Liang, Yuan-Fang Li, Shirui Pan, et al. Time-llm: Time series forecasting by reprogramming large language models. In *International Conference on Learning Representations (ICLR)*, 2024.

Taesung Kim, Jinhee Kim, Yunwon Tae, Cheonbok Park, Jang-Ho Choi, and Jaegul Choo. Reversible instance normalization for accurate time-series forecasting against distribution shift. In *International Conference on Learning Representations (ICLR)*, 2021.

Marcel Kollovieh, Abdul Fatir Ansari, Michael Bohlke-Schneider, Jasper Zschiegner, Hao Wang, and Yuyang Bernie Wang. Predict, refine, synthesize: Self-guiding diffusion models for probabilistic time series forecasting. In *Conference on Neural Information Processing Systems (NeurIPS)*, 2023.

Zhifeng Kong and Wei Ping. On fast sampling of diffusion probabilistic models. *arXiv preprint arXiv:2106.00132*, 2021.

Vincent Le Guen and Nicolas Thome. Shape and time distortion loss for training deep time series forecasting models. In *Conference on Neural Information Processing Systems (NeurIPS)*, 2019.

Vincent Le Guen and Nicolas Thome. Probabilistic time series forecasting with shape and temporal diversity. In *Conference on Neural Information Processing Systems (NeurIPS)*, 2020.

Colin S. Lea, Michael D. Flynn, René Vidal, Austin Reiter, and Gregory Hager. Temporal convolutional networks for action segmentation and detection. In *IEEE / CVF Computer Vision and Pattern Recognition Conference (CVPR)*, 2017.

L. Li, J. Yao, L. K. Wenliang, T. He, T. Xiao, and J. yan. Grin: Generative relation and intention network for multi-agent trajectory prediction. In *Conference on Neural Information Processing Systems (NeurIPS)*, 2021.

Shiyang Li, Xiaoyong Jin, Yao Xuan, Xiyou Zhou, Wenhu Chen, Yu-Xiang Wang, and Xifeng Yan. Enhancing the locality and breaking the memory bottleneck of transformer on time series forecasting. In *Conference on Neural Information Processing Systems (NeurIPS)*, 2019.

Tianhong Li, Yonglong Tian, He Li, Mingyang Deng, and Kaiming He. Autoregressive image generation without vector quantization. In *Conference on Neural Information Processing Systems (NeurIPS)*, 2024a.

Yuxin Li, Wenchao Chen, Xinyue Hu, Bo Chen, Mingyuan Zhou, et al. Transformer-modulated diffusion models for probabilistic multivariate time series forecasting. In *International Conference on Learning Representations (ICLR)*, 2024b.

Shengsheng Lin, Weiwei Lin, Wentai Wu, Feiyu Zhao, Ruichao Mo, and Haotong Zhang. Segrnn: Segment recurrent neural network for long-term time series forecasting. *arXiv preprint arXiv:2308.11200*, 2023.

Shengsheng Lin, Weiwei Lin, Wentai Wu, Haojun Chen, and Junjie Yang. Sparsetsf: Modeling long-term time series forecasting with 1k parameters. In *International Conference on Machine Learning (ICML)*, 2024a.

Shengsheng Lin, Weiwei Lin, Wentai Wu, Songbo Wang, and Yongxiang Wang. Petformer: Long-term time series forecasting via placeholder-enhanced transformer. *IEEE Transactions on Emerging Topics in Computational Intelligence*, 2024b.

Minhao Liu, Ailing Zeng, Muxi Chen, Zhijian Xu, Qiuxia Lai, Lingna Ma, and Qiang Xu. Scinet: Time series modeling and forecasting with sample convolution and interaction. In *Conference on Neural Information Processing Systems (NeurIPS)*, 2022a.

Shizhan Liu, Hang Yu, Cong Liao, Jianguo Li, Weiyao Lin, Alex X. Liu, and Schahram Dustdar. Pyraformer: Low-complexity pyramidal attention for long-range time series modeling and forecasting. In *International Conference on Learning Representations (ICLR)*, 2022b.

Xu Liu, Junfeng Hu, Yuan Li, Shizhe Diao, Yuxuan Liang, Bryan Hooi, and Roger Zimmermann. Unitime: A language-empowered unified model for cross-domain time series forecasting. In *ACM Web Conference (WWW)*, 2024a.

Yong Liu, Tengge Hu, Haoran Zhang, Haixu Wu, Shiyu Wang, Lintao Ma, and Mingsheng Long. itransformer: Inverted transformers are effective for time series forecasting. In *International Conference on Learning Representations (ICLR)*, 2023.

Yong Liu, Haoran Zhang, Chenyu Li, Xiangdong Huang, Jianmin Wang, and Mingsheng Long. Timer: Generative pre-trained transformers are large time series models. In *International Conference on Machine Learning (ICML)*, 2024b.

Donghao Luo and Xue Wang. Moderntcn: A modern pure convolution structure for general time series analysis. In *International Conference on Learning Representations (ICLR)*, 2024.

Meinard Müller. Dynamic time warping. *Information retrieval for music and motion*, 2007.

Alexander Quinn Nichol and Prafulla Dhariwal. Improved denoising diffusion probabilistic models. In *International Conference on Machine Learning (ICML)*, 2021.

Yuqi Nie, Nam H. Nguyen, Phanwadee Sinthong, and Jayant Kalagnanam. A time series is worth 64 words: Long-term forecasting with transformers. In *International Conference on Learning Representations (ICLR)*, 2023.

William Peebles and Saining Xie. Scalable diffusion models with transformers. In *IEEE / CVF Computer Vision and Pattern Recognition Conference (CVPR)*, 2023.

Kashif Rasul, Calvin Seward, Ingmar Schuster, and Roland Vollgraf. Autoregressive denoising diffusion models for multivariate probabilistic time series forecasting. In *International Conference on Machine Learning (ICML)*, 2021a.

Kashif Rasul, Abdul-Saboor Sheikh, Ingmar Schuster, Urs Bergmann, and Roland Vollgraf. Multivariate probabilistic time series forecasting via conditioned normalizing flows. In *International Conference on Learning Representations (ICLR)*, 2021b.

Kashif Rasul, Arjun Ashok, Andrew Robert Williams, Arian Khorasani, George Adamopoulos, Rishika Bhagwatkar, Marin Biloš, Hena Ghonia, Nadhir Hassen, Anderson Schneider, et al. Lag-llama: Towards foundation models for time series forecasting. In *R0-FoMo: Workshop on Robustness of Few-shot and Zero-shot Learning in Foundation Models at NeurIPS*, 2023.

David Salinas, Valentin Flunkert, Jan Gasthaus, and Tim Januschowski. Deepar: Probabilistic forecasting with autoregressive recurrent networks. *International journal of forecasting*, 2020.

Lifeng Shen and James Kwok. Non-autoregressive conditional diffusion models for time series prediction. In *International Conference on Machine Learning (ICML)*, 2023.

Yusuke Tashiro, Jiaming Song, Yang Song, and Stefano Ermon. Csdi: Conditional score-based diffusion models for probabilistic time series imputation. In *Conference on Neural Information Processing Systems (NeurIPS)*, 2021.

Ruey S Tsay. *Analysis of financial time series*. John wiley & sons, 2005.

E Vijay, Arindam Jati, Nam Nguyen, Gift Sinthong, and Jayant Kalagnanam. Tsmixer: Lightweight mlp-mixer model for multivariate time series forecasting. In *ACM SIGKDD International Conference on Knowledge Discovery & Data Mining (KDD)*, 2023.

Qingsong Wen, Tian Zhou, Chaoli Zhang, Weiqi Chen, Ziqing Ma, Junchi Yan, and Liang Sun. Transformers in time series: A survey. 2023.

Gerald Woo, Chenghao Liu, Akshat Kumar, Caiming Xiong, Silvio Savarese, and Doyen Sahoo. Unified training of universal time series forecasting transformers. In *International Conference on Machine Learning (ICML)*, 2024.

Haixu Wu, Jiehui Xu, Jianmin Wang, and Mingsheng Long. Autoformer: Decomposition transformers with auto-correlation for long-term series forecasting. In *Conference on Neural Information Processing Systems (NeurIPS)*, 2021.

Haixu Wu, Tengge Hu, Yong Liu, Hang Zhou, Jianmin Wang, and Mingsheng Long. Timesnet: Temporal 2d-variation modeling for general time series analysis. In *International Conference on Learning Representations (ICLR)*, 2023.

Jinsung Yoon, Daniel Jarrett, and Mihaela Van der Schaar. Time-series generative adversarial networks. In *Conference on Neural Information Processing Systems (NeurIPS)*, 2019.

Chengqing Yu, Fei Wang, Zezhi Shao, Tao Sun, Lin Wu, and Yongjun Xu. Dsformer: A double sampling transformer for multivariate time series long-term prediction. In *Conference on Information and Knowledge Management (CIKM)*, 2023.

Xinyu Yuan and Yan Qiao. Diffusion-ts: Interpretable diffusion for general time series generation. In *International Conference on Learning Representations (ICLR)*, 2024.

Ailing Zeng, Muxi Chen, Lei Zhang, and Qiang Xu. Are transformers effective for time series forecasting? In *AAAI Conference on Artificial Intelligence (AAAI)*, 2023.

Yitian Zhang, Liheng Ma, Soumyasundar Pal, Yingxue Zhang, and Mark Coates. Multi-resolution time-series transformer for long-term forecasting. In *International Conference on Artificial Intelligence and Statistics (AISTATS)*, 2024a.

Yunhao Zhang and Junchi Yan. Crossformer: Transformer utilizing cross-dimension dependency for multivariate time series forecasting. In *International Conference on Learning Representations (ICLR)*, 2023.

Yunhao Zhang, Minghao Liu, Shengyang Zhou, and Junchi Yan. UP2ME: Univariate pre-training to multivariate fine-tuning as a general-purpose framework for multivariate time series analysis. In *International Conference on Machine Learning (ICML)*, 2024b.

Zhenwei Zhang, Xin Wang, and Yuantao Gu. Sageformer: Series-aware graph-enhanced transformers for multivariate time series forecasting. *arXiv preprint arXiv:2307.01616*, 2023.

Haoyi Zhou, Shanghang Zhang, Jieqi Peng, Shuai Zhang, Jianxin Li, Hui Xiong, and Wan Zhang. Informer: Beyond efficient transformer for long sequence time-series forecasting. In *AAAI Conference on Artificial Intelligence (AAAI)*, 2021.

Tian Zhou, Ziqing Ma, Qingsong Wen, Xue Wang, Liang Sun, and Rong Jin. Fedformer: Frequency enhanced decomposed transformer for long-term series forecasting. In *International Conference on Machine Learning (ICML)*, 2022.

Tian Zhou, Peisong Niu, Liang Sun, Rong Jin, et al. One fits all: Power general time series analysis by pretrained lm. In *Conference on Neural Information Processing Systems (NeurIPS)*, 2023.

A Related Works

Backbones for TS Forecasting. Early works employ RNNs (Flunkert et al., 2017) and CNNs (Lea et al., 2017) as backbones. Transformers for TS were introduced later, incorporating techniques such as sparse attention (Li et al., 2019; Zhou et al., 2021), trend-season decomposition (Wu et al., 2021), frequency enhancement (Zhou et al., 2022) and hierarchical structure (Liu et al., 2022b). Nie et al. (2023); Zhang & Yan (2023) proposed patch-based Transformers that divide time series into patches. This approach was later adopted widely, resulting in the development of various patch-based models (Vijay et al., 2023; Lin et al., 2023; Luo & Wang, 2024; Zhang et al., 2023; Yu et al., 2023; Zhang et al., 2024a). Furthermore, many recent pre-training models (Zhang et al., 2024b; Woo et al., 2024; Goswami et al., 2024; Liu et al., 2024b) and cross-modality models (Liu et al., 2024a; Zhou et al., 2023; Jin et al., 2024) also adopt patch-based backbones. Other studies have explored lightweight designs (Zeng et al., 2023; Lin et al., 2024a) and cross-channel dependency capture (Liu et al., 2023; Huang et al., 2023). Despite such advances in backbones, they mostly use regression loss functions. This greatly limits the backbones' capability, especially in diverse forecasting.

Loss Functions for TS Forecasting. Despite extensive research on backbones, limited focus was paid to forecasting specific losses. A line of works uses Dynamic Time Warping (DTW) (Müller, 2007), which computes the similarity between two series with dynamic programming. Cuturi & Blondel (2017) makes DTW differentiable. Le Guen & Thome (2019; 2020) extend DTW to evaluate shape and temporal distortions. However, it is hard to scale non-parallelizable DTW-based losses to long-term tasks. Another line predicts future distributions by estimating their parameters. Common distributions include Student-T (Rasul et al., 2023), Gaussian and negative binomial (Salinas et al., 2020). Additionally, Woo et al. (2024) mix multiple parametric distributions (e.g., Gaussian, Log-normal, etc.) via a Softmax layer. However, these methods rely on predefined formulations, failing to capture complex patterns.

Deep Generative Models for TS. Pioneering efforts on deep generative models for TS include GANs (Yoon et al., 2019), normalizing flows (Rasul et al., 2021b) and VAEs (Li et al., 2021). With the success of diffusion models (Ho et al., 2020; Peebles & Xie, 2023), many diffusion models for TS have also been proposed. Rasul et al. (2021a) propose an RNN-based diffusion model. Tashiro et al. (2021); Alcaraz & Strodthoff (2022) condition diffusion on observed data for imputation. Shen & Kwok (2023) and Li et al. (2024b) respectively use the prediction of autoregressive models and Transformers as the prior knowledge to guide diffusion. Yuan & Qiao (2024) introduces trend-season decomposition to enhance diffusion. These efforts primarily focus on refining denoising networks or optimizing the diffusion process. In contrast, our approach leverages diffusion models to develop a backbone-agnostic loss function.

B Details of AdaLN-MLP

The AdaLN-MLP is an MLP that takes a noisy patch $\mathbf{p}$ and the condition vector $\mathbf{c}$ as input and predicts the noise in $\mathbf{p}$. It is originally a component of Diffusion Transformer (Peebles & Xie, 2023). The Diffusion Transformer was designed to replace the U-Net backbone in diffusion models, and it introduced Adaptive LayerNorm (AdaLN) blocks to inject conditions into diffusion models. One AdaLN block consists of an AdaLN-Attention block and an AdaLN-MLP block. For efficiency, we only use the AdaLN-MLP in our MMPD loss. The computation process of one AdaLN-MLP block is as follows:

$$\begin{aligned} \mathbf{z}^{(s)} &= \mathbf{z}^{(s-1)} + \boldsymbol{\alpha}^{(s)}_{\text{gate}} \circ \text{MLP}\left(\text{AdaLN}(\mathbf{z}^{(s-1)}, \boldsymbol{\gamma}^{(s)}_{\text{scale}}, \boldsymbol{\beta}^{(s)}_{\text{shift}})\right) \\ \text{AdaLN}(\mathbf{z}, \boldsymbol{\gamma}, \boldsymbol{\beta}) &= (1+\boldsymbol{\gamma}) \circ \text{LayerNorm}(\mathbf{z}) + \boldsymbol{\beta} \\ \boldsymbol{\alpha}^{(s)}_{\text{gate}} = \mathbf{W}^{(s)}_{\text{gate}}\phi(\mathbf{c}), &\quad \boldsymbol{\gamma}^{(s)}_{\text{scale}} = \mathbf{W}^{(s)}_{\text{scale}}\phi(\mathbf{c}), \quad \boldsymbol{\beta}^{(s)}_{\text{shift}} = \mathbf{W}^{(s)}_{\text{shift}}\phi(\mathbf{c}) \end{aligned} \tag{12}$$

$\mathbf{z}^{(s)} \in \mathbb{R}^{d_{model}}$ is the output of s-th block (with $\mathbf{z}^{(0)}$ being the linearly embedded $\mathbf{p}$) and $\mathbf{c} \in \mathbb{R}^{d_{model}}$ is the condition. $\circ$ denotes the element-wise product and $\text{MLP}(\cdot)$ is the standard multilayer perceptron. $\boldsymbol{\alpha}^{(s)}_{\text{gate}}, \boldsymbol{\gamma}^{(s)}_{\text{scale}}, \boldsymbol{\beta}^{(s)}_{\text{shift}} \in \mathbb{R}^{d_{model}}$ are parameters to adjust the layer norm and they are obtained by projecting the condition $\phi(\mathbf{c})$ with $\mathbf{W}^{(s)}_{\text{gate}}, \mathbf{W}^{(s)}_{\text{scale}}, \mathbf{W}^{(s)}_{\text{shift}} \in \mathbb{R}^{d_{model} \times d_{model}}$ respectively, where $\phi(\cdot)$ is the activation function. Passing through S AdaLN-MLP blocks, $\mathbf{z}^{(S)}$ is used to make the final

prediction by:

$$\begin{aligned}\hat{\epsilon} &= \mathbf{W}^{(\text{final})}\text{AdaLN}(\mathbf{z}^{(S)}, \boldsymbol{\gamma}^{(\text{out})}_{\text{scale}}, \boldsymbol{\beta}^{(\text{out})}_{\text{shift}}) \\ \boldsymbol{\gamma}^{(\text{out})}_{\text{scale}} &= \mathbf{W}^{(\text{out})}_{\text{scale}}\phi(\mathbf{c}), \quad \boldsymbol{\beta}^{(\text{out})}_{\text{shift}} = \mathbf{W}^{(\text{out})}_{\text{shift}}\phi(\mathbf{c})\end{aligned} \tag{13}$$

where $\mathbf{W}^{(\text{final})} \in \mathbb{R}^{P\times d_{model}}$ and $\mathbf{W}^{(\text{out})}_{\text{scale}}, \mathbf{W}^{(\text{out})}_{\text{shift}} \in \mathbb{R}^{d_{model}\times d_{model}}$.

C Derivation of Multi-Mode Inference Algorithm

To leverage the prior knowledge from forward diffusion, we set the following prior at step k:

$$\begin{aligned}q(\mathbf{Y}^k|\mathbf{Z}^k, \boldsymbol{\mu}^k, \boldsymbol{\Lambda}^k) &= \prod_{n=1}^{N}\prod_{m=1}^{M}\mathcal{N}(\mathbf{y}^k_n; \boldsymbol{\mu}^k_m, (\Lambda^k_m)^{-1}\mathbf{I})^{z^k_{nm}} \\ q(\mathbf{Z}^k|\mathbf{w}^k) &= \prod_{n=1}^{N}\prod_{m=1}^{M}(w^k_m)^{z^k_{nm}} \\ q(\mathbf{w}^k) &= \text{Dirichlet}(\mathbf{w}^k; \boldsymbol{\pi}), \pi_m = \rho^{m-1} \\ q(\boldsymbol{\Lambda}^k) &= \prod_{m=1}^{M}\text{Gamma}(\Lambda^k_m; u^k_m, v^k_m) \\ u^k_m &= u, v^k_m = u * (1-\bar{\alpha}_k)\end{aligned} \tag{14}$$

Note that we use $q(\cdot)$ to denote prior distributions and $\{\pi^k_m, u^k_m, v^k_m\}_{m=1}^M$ without tilde for parameters in prior distributions. $p(\cdot)$ are for posterior distributions and $\{\widetilde{\pi}^k_m, \widetilde{u}^k_m, \widetilde{v}^k_m\}_{m=1}^M$ for parameters in posterior distributions.

With the above priors, we get the joint distribution $q(\mathbf{Y}^k, \mathbf{Z}^k, \mathbf{w}^k, \boldsymbol{\Lambda}^k|\boldsymbol{\mu}^k) = q(\mathbf{Y}^k|\mathbf{Z}^k, \boldsymbol{\mu}^k, \boldsymbol{\Lambda}^k)q(\mathbf{Z}^k|\mathbf{w}^k)q(\mathbf{w}^k)q(\boldsymbol{\Lambda}^k)$. Obtaining samples at step k, $\mathbf{Y}^k = \{\mathbf{y}^k_n\}_{n=1}^N$, our goal is to maximize the marginal log probability $\max_{\boldsymbol{\mu}^k}\ln q(\mathbf{Y}^k|\boldsymbol{\mu}^k)$ and get the posterior distribution $q(\mathbf{Z}^k, \mathbf{w}^k, \boldsymbol{\Lambda}^k|\mathbf{Y}^k, \boldsymbol{\mu}^k_{opt})$, where $\boldsymbol{\mu}^k_{opt}$ denotes optimal parameters. It is hard to directly optimize the marginal distribution and obtain the posterior as they both contain complex integral terms. Therefore, we introduce variational distribution $p(\mathbf{Z}^k, \mathbf{w}^k, \boldsymbol{\Lambda}^k)$ to approximate the posterior through variational inference (Bishop & Nasrabadi, 2006). To maximize $\max_{\boldsymbol{\mu}^k}\ln q(\mathbf{Y}^k|\boldsymbol{\mu}^k)$ and approximate posterior $q(\mathbf{Z}^k, \mathbf{w}^k, \boldsymbol{\Lambda}^k|\mathbf{Y}^k, \boldsymbol{\mu}^k)$ with $p(\mathbf{Z}^k, \mathbf{w}^k, \boldsymbol{\Lambda}^k)$, we get the following objective:

$$\begin{aligned}&\max_{\boldsymbol{\mu}^k, p^k} \quad \ln q(\mathbf{Y}^k|\boldsymbol{\mu}^k) - \text{KL}[p(\mathbf{Z}^k, \mathbf{w}^k, \boldsymbol{\Lambda}^k)||q(\mathbf{Z}^k, \mathbf{w}^k, \boldsymbol{\Lambda}^k|\mathbf{Y}^k, \boldsymbol{\mu}^k)] \\ =&\max_{\boldsymbol{\mu}^k, p^k} \quad \int p(\mathbf{Z}^k, \mathbf{w}^k, \boldsymbol{\Lambda}^k)\left[\ln q(\mathbf{Y}^k|\boldsymbol{\mu}^k) - \ln\frac{p(\mathbf{Z}^k, \mathbf{w}^k, \boldsymbol{\Lambda}^k)}{q(\mathbf{Z}^k, \mathbf{w}^k, \boldsymbol{\Lambda}^k|\mathbf{Y}^k, \boldsymbol{\mu}^k)}\right]d\mathbf{Z}^k d\mathbf{w}^k d\boldsymbol{\Lambda}^k \\ =&\max_{\boldsymbol{\mu}^k, p^k} \quad \int p(\mathbf{Z}^k, \mathbf{w}^k, \boldsymbol{\Lambda}^k)\ln\frac{q(\mathbf{Y}^k, \mathbf{Z}^k, \mathbf{w}^k, \boldsymbol{\Lambda}^k|\boldsymbol{\mu}^k)}{p(\mathbf{Z}^k, \mathbf{w}^k, \boldsymbol{\Lambda}^k)}d\mathbf{Z}^k d\mathbf{w}^k d\boldsymbol{\Lambda}^k \\ =&\max_{\boldsymbol{\mu}^k, p^k} \quad \mathcal{L}(\boldsymbol{\mu}^k, p(\mathbf{Z}^k, \mathbf{w}^k, \boldsymbol{\Lambda}^k))\end{aligned} \tag{15}$$

where p^k is short for $p(\mathbf{Z}^k, \mathbf{w}^k, \boldsymbol{\Lambda}^k)$ and $\mathcal{L}(\boldsymbol{\mu}^k, p(\mathbf{Z}^k, \mathbf{w}^k, \boldsymbol{\Lambda}^k))$ is often called Evidence Lower Bound (ELBO) in variational inference. Using mean field approximation, we decompose the variational distribution into $p(\mathbf{Z}^k, \mathbf{w}^k, \boldsymbol{\Lambda}^k) = p(\mathbf{Z}^k)p(\mathbf{w}^k)p(\boldsymbol{\Lambda}^k)$.

Given newly generated samples at step k, $\mathbf{Y}^k$, we maximize $\mathcal{L}(\boldsymbol{\mu}^k, p(\mathbf{Z}^k), p(\mathbf{w}^k), p(\boldsymbol{\Lambda}^k))$ w.r.t $p(\mathbf{Z}^k), \boldsymbol{\mu}^k, p(\mathbf{w}^k), p(\boldsymbol{\Lambda}^k)$ one by one. An advantage of fitting an evolving variational GMM alongside the diffusion process is that we can use well-fitted posteriors, i.e., $p(\mathbf{Z}^{k+1}), \boldsymbol{\mu}^{k+1}, p(\mathbf{w}^{k+1}), p(\boldsymbol{\Lambda}^{k+1})$ at step $k+1$ as the initialization of step k. This is because in diffusion, the difference between samples generated in two adjacent steps $\mathbf{Y}^{k+1}$ and $\mathbf{Y}^k$ is small, and in our setting, the difference between the prior distributions of two adjacent steps is also minimal. As a result, we initialize

$p(\mathbf{Z}^k), \boldsymbol{\mu}^k, p(\mathbf{w}^k), p(\boldsymbol{\Lambda}^k)$ using optimized parameters from last step $k+1$ as the following:

$$\begin{aligned} p(\mathbf{Z}^k) &= \prod_{n=1}^{N}\prod_{m=1}^{M}(\widetilde{\gamma}_{nm}^{k+1})^{z_{nm}^k} \\ \boldsymbol{\mu}^k &= \boldsymbol{\mu}^{k+1} \\ p(\mathbf{w}^k) &= \text{Dirichlet}(\mathbf{w}^k; \widetilde{\boldsymbol{\pi}}^{k+1}) \\ p(\boldsymbol{\Lambda}^k) &= \prod_{m=1}^{M}\text{Gamma}(\Lambda_m^k; \widetilde{u}_m^{k+1}, \widetilde{v}_m^{k+1}) \end{aligned} \tag{16}$$

E-step: Update $p(\mathbf{Z}^k)$. Fixing $\boldsymbol{\mu}^k, p(\mathbf{w}^k), p(\boldsymbol{\Lambda}^k)$, the objective becomes:

$$\begin{aligned} &\max_{p(\mathbf{Z}^k)} \quad \mathcal{L}(\boldsymbol{\mu}^k, p(\mathbf{Z}^k), p(\mathbf{w}^k), p(\boldsymbol{\Lambda}^k)) \\ &= \max_{p(\mathbf{Z}^k)} \quad \int_{\mathbf{Z}^k,\boldsymbol{\Lambda}^k} p(\mathbf{Z}^k)p(\boldsymbol{\Lambda}^k)\ln q(\mathbf{Y}^k|\mathbf{Z}^k,\boldsymbol{\mu}^k,\boldsymbol{\Lambda}^k)d\mathbf{Z}^k d\boldsymbol{\Lambda}^k \\ &\qquad + \int_{\mathbf{Z}^k,\mathbf{w}^k} p(\mathbf{Z}^k)p(\mathbf{w}^k)\ln q(\mathbf{Z}^k|\mathbf{w})d\mathbf{Z}^k d\mathbf{w}^k - \int_{\mathbf{Z}^k} p(\mathbf{Z}^k)\ln p(\mathbf{Z}^k)d\mathbf{Z}^k + \text{Const} \\ &= \min_{p(\mathbf{Z}^k)} \quad \text{KL}[p(\mathbf{Z}^k)||\widetilde{p}(\mathbf{Z}^k)] \end{aligned} \tag{17}$$

where Const denotes constant terms w.r.t $p(\mathbf{Z}^k)$, $\widetilde{p}(\mathbf{Z}^k)$ is a new distribution with:

$$\ln\widetilde{p}(\mathbf{Z}^k) = \mathbb{E}_{p(\boldsymbol{\Lambda}^k)}[\ln q(\mathbf{Y}^k|\mathbf{Z}^k,\boldsymbol{\mu}^k,\boldsymbol{\Lambda}^k)] + \mathbb{E}_{p(\mathbf{w}^k)}[\ln q(\mathbf{Z}^k|\mathbf{w}^k)] + \text{Const} \tag{18}$$

Therefore, KL divergence is minimized when $p(\mathbf{Z}^k) = \widetilde{p}(\mathbf{Z}^k)$:

$$\begin{aligned} &\ln p(\mathbf{Z}^k) = \ln\widetilde{p}(\mathbf{Z}^k) \\ &= \mathbb{E}_{p(\boldsymbol{\Lambda}^k)}[\sum_{n=1}^{N}\sum_{m=1}^{M} z_{nm}^k \ln\mathcal{N}(\mathbf{y}_n^k; \boldsymbol{\mu}_m^k, (\Lambda_m^k)^{-1}\mathbf{I})] + \mathbb{E}_{p(\mathbf{w}^k)}[\sum_{n=1}^{N}\sum_{m=1}^{M} z_{nm}^k \ln w_m^k] + \text{Const} \\ &= \sum_{n=1}^{N}\sum_{m=1}^{M} z_{nm}^k \ln\gamma_{nm}^k + \text{Const} \end{aligned} \tag{19}$$

where

$$\begin{aligned} \ln\gamma_{nm}^k = &-\frac{1}{2}\left[\frac{\widetilde{u}_m^{k+1}}{\widetilde{v}_m^{k+1}}\|\mathbf{y}_n^k - \boldsymbol{\mu}_m^{k+1}\|_2^2 + \tau\ln(2\pi)\right] + \frac{\tau}{2}\left[\psi(\widetilde{u}_m^{k+1}) - \ln(\widetilde{v}_m^{k+1})\right] \\ &+ \psi(\widetilde{\pi}_m^{k+1}) - \psi(\sum_{s=1}^{M}\widetilde{\pi}_s^{k+1}) \end{aligned} \tag{20}$$

Normalizing it, we get the formulation of $p(\mathbf{Z}^k)$:

$$p(\mathbf{Z}^k) = \prod_{n=1}^{N}\prod_{m=1}^{M}(\widetilde{\gamma}_{nm}^k)^{z_{nm}^k}, \quad \widetilde{\gamma}_{nm}^k = \frac{\gamma_{nm}^k}{\sum_{s=1}^{M}\gamma_{ns}^k} \tag{21}$$

which means that the posterior probability of $\mathbf{y}_n^k$ belonging to mode m is $p(z_{nm}^k = 1) = \widetilde{\gamma}_{nm}^k$.

M-step: Update $\boldsymbol{\mu}^k$. Note that $p(\mathbf{Z}^k)$ has already be updated. Fixing $p(\mathbf{Z}^k), p(\mathbf{w}^k), p(\boldsymbol{\Lambda}^k)$, the objective becomes:

$$\begin{aligned} &\max_{\boldsymbol{\mu}^k} \quad \mathcal{L}(\boldsymbol{\mu}^k, p(\mathbf{Z}^k), p(\mathbf{w}^k), p(\boldsymbol{\Lambda}^k)) \\ &= \max_{\boldsymbol{\mu}^k} \quad \int_{\mathbf{Z}^k,\boldsymbol{\Lambda}^k} p(\mathbf{Z}^k)p(\boldsymbol{\Lambda}^k)\ln q(\mathbf{Y}^k|\mathbf{Z}^k,\boldsymbol{\mu}^k,\boldsymbol{\Lambda}^k)d\mathbf{Z}^k d\boldsymbol{\Lambda}^k + \text{Const} \\ &= \max_{\boldsymbol{\mu}^k} \quad \mathbb{E}_{p(\mathbf{Z}^k),p(\boldsymbol{\Lambda}^k)}[\sum_{n=1}^{N}\sum_{m=1}^{M} z_{nm}^k \ln\mathcal{N}(\mathbf{y}_n^k; \boldsymbol{\mu}_m^k, (\Lambda_m^k)^{-1}\mathbf{I})] \\ &= \min_{\boldsymbol{\mu}^k} \quad \sum_{m=1}^{M}\frac{\widetilde{u}_m^{k+1}}{\widetilde{v}_m^{k+1}}\sum_{n=1}^{N}\widetilde{\gamma}_{nm}^k\|\mathbf{y}_n^k - \boldsymbol{\mu}_m^k\|_2^2 \end{aligned} \tag{22}$$

Setting the gradient w.r.t $\boldsymbol{\mu}_m^k$ to zero, we get the updated $\boldsymbol{\mu}^k$:

$$\boldsymbol{\mu}_m^k = \frac{1}{\widetilde{N}_m^k} \sum_{n=1}^{N} \widetilde{\gamma}_{nm}^k \mathbf{y}_n^k, \quad \widetilde{N}_m^k = \sum_{n=1}^{N} \widetilde{\gamma}_{nm}^k \tag{23}$$

M-step: Update $p(\mathbf{w}^k)$. Note that $p(\mathbf{Z}^k), \boldsymbol{\mu}^k$ have already be updated. Similar to E-step, fixing $p(\mathbf{Z}^k), \boldsymbol{\mu}^k, p(\boldsymbol{\Lambda}^k)$, the objective becomes:

$$\begin{aligned} &\max_{p(\mathbf{w}^k)} \quad \mathcal{L}(\boldsymbol{\mu}^k, p(\mathbf{Z}^k), p(\mathbf{w}^k), p(\boldsymbol{\Lambda}^k)) \\ =&\max_{p(\mathbf{w}^k)} \quad \int_{\mathbf{Z}^k, \mathbf{w}^k} p(\mathbf{Z}^k) p(\mathbf{w}^k) \ln q(\mathbf{Z}^k | \mathbf{w}^k) d\mathbf{Z}^k d\mathbf{w}^k \\ &\quad + \int_{\mathbf{w}^k} p(\mathbf{w}^k) \ln q(\mathbf{w}^k) d\mathbf{w}^k - \int_{\mathbf{w}^k} p(\mathbf{w}^k) \ln p(\mathbf{w}^k) d\mathbf{w}^k + \text{Const} \end{aligned} \tag{24}$$

And the log probability of the optimal $p(\mathbf{w}^k)$ should be:

$$\begin{aligned} \ln p(\mathbf{w}^k) &= \mathbb{E}_{p(\mathbf{Z}^k)}[\ln q(\mathbf{Z}^k | \mathbf{w}^k)] + \ln q(\mathbf{w}^k) + \text{Const} \\ &= \sum_{m=1}^{M} (\pi_m + \widetilde{N}_m^k - 1) \ln w_m^k + \text{Const} \end{aligned} \tag{25}$$

Therefore, the updated $p(\mathbf{w}^k)$ is the following Dirichlet distribution:

$$p(\mathbf{w}^k) = \text{Dirichlet}(\mathbf{w}^k; \widetilde{\boldsymbol{\pi}}^k), \quad \widetilde{\pi}_m^k = \pi_m + \widetilde{N}_m^k \tag{26}$$

M-step: Update $p(\boldsymbol{\Lambda}^k)$. Note that $p(\mathbf{Z}^k), \boldsymbol{\mu}^k, p(\mathbf{w}^k)$ have already be updated. Fixing $p(\mathbf{Z}^k), \boldsymbol{\mu}^k, p(\mathbf{w}^k)$, the objective becomes:

$$\begin{aligned} &\max_{p(\boldsymbol{\Lambda}^k)} \quad \mathcal{L}(\boldsymbol{\mu}^k, p(\mathbf{Z}^k), p(\mathbf{w}^k), p(\boldsymbol{\Lambda}^k)) \\ =&\max_{p(\boldsymbol{\Lambda}^k)} \quad \int_{\mathbf{Z}^k, \boldsymbol{\Lambda}^k} p(\mathbf{Z}^k) p(\boldsymbol{\Lambda}^k) \ln q(\mathbf{Y}^k | \mathbf{Z}^k, \boldsymbol{\mu}^k, \boldsymbol{\Lambda}^k) d\mathbf{Z}^k d\boldsymbol{\Lambda}^k \\ &\quad + \int_{\boldsymbol{\Lambda}^k} p(\boldsymbol{\Lambda}^k) \ln q(\boldsymbol{\Lambda}^k) d\boldsymbol{\Lambda}^k - \int_{\boldsymbol{\Lambda}^k} p(\boldsymbol{\Lambda}^k) \ln p(\boldsymbol{\Lambda}^k) d\boldsymbol{\Lambda}^k + \text{Const} \end{aligned} \tag{27}$$

The log probability of the optimal $p(\boldsymbol{\Lambda}^k)$ should be:

$$\begin{aligned} &\ln p(\boldsymbol{\Lambda}^k) \\ =&\mathbb{E}_{p(\mathbf{Z}^k)}[\ln q(\mathbf{Y}^k | \mathbf{Z}^k, \boldsymbol{\mu}^k, \boldsymbol{\Lambda}^k)] + \ln q(\boldsymbol{\Lambda}^k) + \text{Const} \\ =&\sum_{m=1}^{M} \left\{ \left(u_m^k + \frac{\tau}{2} \widetilde{N}_m^k - 1 \right) \ln \Lambda_m^k - \left(v_m^k + \frac{1}{2} \sum_{n=1}^{N} \widetilde{\gamma}_{nm}^k \| \mathbf{y}_n^k - \boldsymbol{\mu}_m^k \|_2^2 \right) \Lambda_m^k \right\} + \text{Const} \end{aligned} \tag{28}$$

which means the updated $p(\boldsymbol{\Lambda}^k)$ is the following Gamma distribution:

$$\begin{aligned} p(\boldsymbol{\Lambda}^k) &= \prod_{m=1}^{M} \text{Gamma}(\Lambda_m^k; \widetilde{u}_m^k, \widetilde{v}_m^k) \\ \widetilde{u}_m^k = u_m^k + \frac{\tau}{2} \widetilde{N}_m^k, &\quad \widetilde{v}_m^k = v_m^k + \frac{1}{2} \sum_{n=1}^{N} \widetilde{\gamma}_{nm}^k \| \mathbf{y}_n^k - \boldsymbol{\mu}_m^k \|_2^2 \end{aligned} \tag{29}$$

Eq. 21,23,26,29 are the resulting four steps in Algorithm 1. As each of the four steps raises $\mathcal{L}(\boldsymbol{\mu}^k, p(\mathbf{Z}^k), p(\mathbf{w}^k), p(\boldsymbol{\Lambda}^k))$, the objective gets greater after one iteration. It is also possible to perform the four-step iteration multiple times at each step k to ensure convergence.

D Detailed Setup of Experiments

D.1 Datasets

We conduct experiments on eight datasets following Nie et al. (2023); Wu et al. (2023). These datasets include:

- **1)ETTh1** and **2)ETTm1**. These two datasets record 7 key indicators of an electricity transformer, such as load and oil temperature. ETTh1 records data points every hour, and ETTm1 records every 15 minutes. The whole datasets cover a period of two years and we use data from the first 20 months and split it into train/validation/test sets with a ratio of 0.6:0.2:0.2.
- **3)ETTh2** and **4)ETTm2**. The contents, formats and data split of these two datasets are similar to those of ETTh1 and ETTm1, but the records are from another electricity transformer.
- **5)WTH.** This dataset contains 21 weather indicators in Beutenberg, including air temperature and dewpoint, with data points recorded every 10 minutes throughout the year 2020. The train/validation/test sets are split with a ratio of 0.7:0.1:0.2.
- **6)ECL.** This dataset records the hourly electricity consumption (in kW) of 321 clients from 2012 to 2014. The train/validation/test sets are split with a ratio of 0.7:0.1:0.2.
- **7)Traffic** This dataset includes road occupancy rates measured by 862 sensors on freeways in the San Francisco Bay area from July 2016 to June 2018, with data points recorded every hour. The train/validation/test sets are split with a ratio of 0.7:0.1:0.2.
- **8)Dynamic.** This dataset consists of 17 sensors reading and control signals of a simulated complex dynamical system, with data points recorded every second. The original dataset is from `https://www.kaggle.com/datasets/patrickfleith/dynamical-system-multivariate-time-series-forecast` and contains 5,000,000 timestamps. For training time concerns, we use the first 10% data, which corresponds to 500,000 timestamps, and split it into train/validation/test sets with a ratio of 0.7:0.1:0.2. It is worth noting that, despite using only 10% of the original data, the selected timestamps still far exceed those in the previous seven datasets.

The first seven datasets are widely used datasets for TS forecasting (Nie et al., 2023; Wu et al., 2023). In line with standard protocol, we use the last $T = 336$ steps to predict the next $\tau = \{96, 192, 336, 720\}$ steps. To evaluate model performance in more complex scenarios, we introduce a new dataset, Dynamic, which has more complex patterns with no obvious periodicity. For Dynamic, we use the last $T = 600$ steps (10 minutes) to predict the next $\tau = \{60, 120, 180, 300\}$ steps (corresponding to $\{1, 2, 3, 5\}$ minutes). Additionally, due to the large scale of Dynamic, we divide its test set into non-overlapping windows by setting the sliding window step equal to τ. In contrast, for the other datasets, we generate overlapping windows with a sliding step of 1, following the common protocol. Detailed statistical characteristics of the used datasets are shown in Table 6.

Table 6: Statistical characteristics of datasets

Dataset	#Channels	#Timestamps	Split	T	τ	Field
ETTh1	7	14,400	0.6:0.2:0.2	336	{96, 192, 336, 720}	Electricity Transformer
ETTm1	7	57,600	0.6:0.2:0.2	336	{96, 192, 336, 720}	Electricity Transformer
ETTh2	7	14,400	0.6:0.2:0.2	336	{96, 192, 336, 720}	Electricity Transformer
ETTm2	7	57,600	0.6:0.2:0.2	336	{96, 192, 336, 720}	Electricity Transformer
WTH	21	52,696	0.7:0.1:0.2	336	{96, 192, 336, 720}	Meteorological Indicators
ECL	321	26,304	0.7:0.1:0.2	336	{96, 192, 336, 720}	Electricity Consumption
Traffic	862	17,544	0.7:0.1:0.2	336	{96, 192, 336, 720}	Road Occupancy
Dynamic	17	500,000	0.7:0.1:0.2	600	{60, 120, 180, 300}	Complex Dynamical System

D.2 METRICS

Top-K MSE. The ground truth target is $\mathbf{y} \in \mathbb{R}^\tau$. Multi-mode predictions are $\{\widetilde{\mathbf{y}}_m\}_{m=1}^M, \mathbf{y}_m \in \mathbb{R}^\tau$ and corresponding probabilities are $\{w_m\}_{m=1}^M, \sum_{m=1}^M w_m = 1$. Top-K MSE is computed as:

$$\begin{aligned} \mathcal{M} &= \textbf{Top-K}(\{w_m\}_{m=1}^M) \\ \forall m \in \mathcal{M}, \text{MSE}_m &= \frac{1}{\tau}\|\widetilde{\mathbf{y}}_m - \mathbf{y}\|_2^2 \\ \text{Top-K MSE} &= \min_{m \in \mathcal{M}} \text{MSE}_m \end{aligned} \tag{30}$$

We first pick the Top-K modes with the highest probabilities into $\mathcal{M}$. Then MSE of each mode in $\mathcal{M}$ is computed. Finally, the minimum MSE among the selected K mode is reported as Top-K MSE.

Top-K MAE. The computation of Top-K MAE is similar to Top-K MSE, with MSE changing to MAE:

$$\begin{aligned} \mathcal{M} &= \textbf{Top-K}(\{w_m\}_{m=1}^M) \\ \forall m \in \mathcal{M}, \text{MAE}_m &= \frac{1}{\tau}\|\widetilde{\mathbf{y}}_m - \mathbf{y}\|_1 \\ \text{Top-K MAE} &= \min_{m \in \mathcal{M}} \text{MAE}_m \end{aligned} \tag{31}$$

MSE. Given ground truth target $\mathbf{y} \in \mathbb{R}^\tau$ and deterministic prediction $\widetilde{\mathbf{y}} \in \mathbb{R}^\tau$, MSE is computed as:

$$\text{MSE} = \frac{1}{\tau}\|\widetilde{\mathbf{y}} - \mathbf{y}\|_2^2 \tag{32}$$

CRPS. CRPS is a frequently used metric for probabilistic prediction and it is originally defined for the scaler variable. Given the ground truth target $y \in \mathbb{R}$ and the cumulative distribution function (CDF) of the predicted distribution $\widetilde{F}(y)$, the CRPS is defined as:

$$\text{CRPS}(\widetilde{F}, y) = \int_{-\infty}^{+\infty} \left(\widetilde{F}(\widetilde{y}) - \mathbb{1}(\widetilde{y} \geq y)\right)^2 d\widetilde{y} \tag{33}$$

Gneiting & Raftery (2007) show that CRPS can also be computed by:

$$\text{CRPS}(\widetilde{F}, y) = \mathbb{E}_{\widetilde{y}}\left[|\widetilde{y} - y|\right] - \frac{1}{2}\mathbb{E}_{\widetilde{y}, \widetilde{y}^*}\left[|\widetilde{y} - \widetilde{y}^*|\right] \tag{34}$$

where $\widetilde{y}, \widetilde{y}^*$ are random variables following the predicted distribution, i.e., distribution corresponding to $\widetilde{F}(y)$.

Following this formulation, given the ground truth target $\mathbf{y} \in \mathbb{R}^\tau$ and samples draw from the probabilistic model $\{\widetilde{\mathbf{y}}_i\}_{i=1}^N, \mathbf{y}_i \in \mathbb{R}^\tau$, we compute the CRPS by:

$$\begin{aligned} \text{CRPS}_t &\approx \frac{1}{N}\sum_{i=1}^N |\widetilde{y}_{i,t} - y_t| - \frac{1}{2N^2}\sum_{i=1}^N\sum_{j=1}^N |\widetilde{y}_{i,t} - \widetilde{y}_{j,t}| \\ \text{CRPS} &= \frac{1}{\tau}\sum_{t=1}^\tau \text{CRPS}_t \end{aligned} \tag{35}$$

where $\widetilde{y}_{i,t} \in \mathbb{R}$ is the predicted value of timestamp t in sample $\widetilde{\mathbf{y}}_i$. $y_t \in \mathbb{R}$ is the target at timestamp t. We approximate the CRPS at each step and use the average across steps as the CRPS of the whole series.

Remark. CRPS also has the following connection with quantile loss:

$$\begin{aligned} \text{CRPS}(\widetilde{F}, y) &= 2\int_0^1 \rho_\alpha(y - \widetilde{F}^{-1}(\alpha))d\alpha \\ \rho_\alpha(u) &= u(\alpha - \mathbb{1}(u < 0)) \end{aligned} \tag{36}$$

As a result, some works (Woo et al., 2024) approximate CRPS_t by:

$$\text{CRPS}_t \approx \frac{2}{K} \sum_{k=1}^{K} \rho_{\alpha_k} \left(y_t - Q(\{\widetilde{y}_{i,t}\}_{i=1}^{N}, \alpha_k) \right) \tag{37}$$

where $Q(\{\widetilde{y}_{i,t}\}_{i=1}^{N}, \alpha_k)$ computes the α_k-quantile at step t. $\{\alpha_k\}_{k=1}^{K}$ are some pre-defined quantiles for integral approximation. We do not use this approximation because it will be affected by the selection of $\{\alpha_k\}_{k=1}^{K}$ and the quantile function $Q(\cdot)$.

We have described the metrics for a univariate instance. Since all the datasets we used are multivariate, we compute the metrics for each channel and then average them across channels to obtain the metrics for a multivariate instance. Finally, the metrics for a dataset are calculated by averaging the metrics across all instances in the test set.

D.3 Implementations

The default patch size is set to $P = 12$. For the sake of saving runtime memory, we use $P = 24$ at $\tau = \{336, 720\}$ or when the dataset is ECL or Traffic. As for the Patch Consistent MLP, we use a one-block MLP with the dimension of hidden states $d_{model} = 256$, adjacent range hyper-parameter $r = 3$ on all datasets.

Regarding the training process, we use a linear noise schedule with $K_{train} = 1,000$ diffusion steps (Ho et al., 2020). The default diffusion-deterministic balancing weight, i.e., λ in Eq. 8, is set to 0.99. When using SegRNN as the backbone, it is set to 0.9. Adam optimizer with a learning rate of 1e-4 is used for optimization. The maximum number of training epochs is set to 20, and if the validation loss does not decrease over 5 consecutive validations, the training process is terminated early. The commonly used instance normalization (Kim et al., 2021) is also applied to reduce the distribution shift.

As for inference, for each input, we generate $N = 100$ samples and set the maximum number of modes to $M = 10$. In our multi-mode inference algorithm, we resample the inference-time diffusion steps to $K_{infer} = 20$ and perform 10 EM iterations at each step. The hyper-parameters are set to $\rho = 0.5, u = 100$. For other baselines, we draw N samples from their corresponding distributions and post-process them with a GMM in the same formulation as in MMPD to obtain multi-mode predictions.

All models are implemented in Pytorch and run on NVIDIA GeForce RTX 3090 GPUs with 24GB memory.

E Full Results

Due to space limitations in the main text, we present the full results from Sec. 4.1 here. Table 7 shows the Top-3 MSE, Top-3 MAE, MSE and CRPS evaluations of different loss functions across various forecasting horizons τ. Table 8 displays the Top-3 MSE and Top-3 MAE evaluations for MSE, Mix, and MMPD across three different backbones at different forecasting horizons. Finally, Table 9 presents the MSE and CRPS evaluations across three different backbones at different forecasting horizons.

Table 7: Full Top-3 MSE, Top-3 MAE, MSE and CRPS evaluations of different loss functions on different forecasting horizons τ, which is set to $\{96, 192, 336, 720\}$ for the first seven datasets and $\{60, 120, 180, 300\}$ for Dynamic. "Gauss" is short for "Gaussian". "T" is short for "Student-T". Bold/underline indicates the best/second. Our method is marked in gray. Inf indicates the infinity problem caused by outliers.

Metric		Top-3 MSE						Top-3 MAE						MSE						CRPS					
Loss		MSE	MAE	Gauss	T	Mix	MMPD	MSE	MAE	Gauss	T	Mix	MMPD	MSE	MAE	Gauss	T	Mix	MMPD	MSE	MAE	Gauss	T	Mix	MMPD
ETTh1	96	0.365	0.390	0.381	0.375	0.371	**0.329**	0.399	0.395	0.400	0.391	0.382	**0.371**	**0.374**	0.385	0.383	0.377	0.399	0.375	0.316	0.325	0.291	**0.283**	0.286	0.289
	192	0.412	0.425	0.429	0.415	0.411	**0.396**	0.426	0.422	0.427	0.415	0.419	**0.405**	0.411	0.415	0.426	0.413	0.426	**0.406**	0.331	0.338	0.311	**0.300**	0.311	0.314
	336	0.446	0.450	0.447	0.458	**0.410**	0.415	0.449	0.444	0.444	0.442	**0.419**	0.422	0.436	0.439	0.440	0.454	0.449	**0.422**	0.342	0.349	0.320	0.322	**0.314**	0.326
	720	0.496	0.501	0.501	0.470	0.510	**0.445**	0.488	0.486	0.476	0.463	0.486	**0.453**	0.481	0.488	0.488	0.462	0.511	**0.444**	0.361	0.371	0.345	**0.333**	0.353	0.340
	Avg	0.430	0.441	0.439	0.430	0.425	**0.396**	0.440	0.437	0.437	0.428	0.426	**0.412**	0.425	0.432	0.434	0.426	0.446	**0.412**	0.337	0.346	0.317	**0.310**	0.316	0.318
ETTm1	96	0.265	0.309	0.291	0.284	0.188	**0.180**	0.333	0.336	0.344	0.327	0.277	**0.272**	0.290	0.307	0.297	0.287	0.303	**0.280**	0.281	0.291	0.253	0.242	**0.239**	**0.239**
	192	0.317	0.344	0.340	0.333	0.253	**0.240**	0.364	0.363	0.375	0.358	0.321	**0.314**	0.323	0.334	0.338	0.331	0.337	**0.315**	0.296	0.304	0.274	0.261	**0.258**	0.259
	336	0.368	0.371	0.370	0.364	0.320	**0.291**	0.393	0.385	0.393	0.381	0.354	**0.348**	0.360	0.359	0.364	0.359	0.371	**0.352**	0.311	0.316	0.284	**0.276**	**0.276**	0.280
	720	0.441	0.433	0.444	0.426	0.397	**0.367**	0.435	0.419	0.432	0.418	0.398	**0.392**	0.427	0.420	0.430	0.419	0.423	**0.401**	0.338	0.339	0.317	0.304	0.304	**0.303**
	Avg	0.348	0.364	0.361	0.352	0.289	**0.269**	0.381	0.375	0.386	0.371	0.338	**0.331**	0.350	0.355	0.357	0.349	0.358	**0.337**	0.307	0.313	0.282	0.271	**0.269**	0.270
ETTh2	96	0.273	0.293	0.285	0.305	0.260	**0.241**	0.334	0.336	0.347	0.343	0.328	**0.310**	0.294	0.296	0.305	0.304	0.322	**0.293**	0.264	0.263	0.271	**0.261**	0.271	0.271
	192	0.345	0.360	0.363	0.364	0.320	**0.283**	0.382	0.382	0.395	0.385	0.371	**0.344**	0.367	0.358	0.377	0.361	0.401	**0.357**	0.299	**0.291**	0.305	0.292	0.309	0.294
	336	0.391	0.408	0.419	0.403	0.363	**0.310**	0.414	0.416	0.433	0.416	0.393	**0.368**	0.399	0.404	0.419	0.400	0.402	**0.366**	0.318	0.315	0.329	0.316	0.318	**0.312**
	720	0.448	0.411	0.450	0.430	0.430	**0.360**	0.463	0.433	0.469	0.448	0.454	**0.407**	0.444	0.408	0.430	0.423	0.437	**0.400**	0.350	**0.326**	0.355	0.332	0.343	0.329
	Avg	0.364	0.368	0.379	0.375	0.343	**0.299**	0.398	0.392	0.411	0.398	0.387	**0.357**	0.376	0.366	0.382	0.372	0.390	**0.354**	0.308	**0.299**	0.315	0.300	0.310	0.301
ETTm2	96	0.156	0.174	0.176	0.180	0.156	**0.135**	0.244	0.253	0.270	0.258	0.242	**0.224**	**0.169**	0.174	0.194	0.180	0.179	0.173	0.196	0.200	0.211	0.194	0.193	**0.192**
	192	0.223	0.241	0.233	0.248	0.203	**0.185**	0.293	0.298	0.307	0.305	0.279	**0.266**	0.234	0.238	0.243	0.246	0.244	**0.227**	0.229	0.230	0.235	0.230	0.226	**0.225**
	336	0.293	0.301	0.308	0.322	0.259	**0.225**	0.342	0.338	0.356	0.364	0.319	**0.294**	0.298	0.298	0.306	0.317	0.318	**0.289**	0.261	0.258	0.269	0.270	0.262	**0.255**
	720	0.383	0.387	0.403	0.395	0.362	**0.313**	0.399	0.397	0.417	0.407	0.393	**0.357**	0.379	0.384	0.393	0.390	0.399	**0.367**	0.304	0.301	0.310	0.305	0.309	**0.298**
	Avg	0.264	0.276	0.280	0.286	0.245	**0.214**	0.320	0.321	0.337	0.333	0.308	**0.285**	0.270	0.274	0.284	0.283	0.285	**0.264**	0.247	0.247	0.256	0.250	0.247	**0.243**
WTH	96	0.142	0.153	0.156	0.157	0.144	**0.121**	0.192	0.193	0.207	0.193	0.183	**0.155**	**0.149**	0.153	0.166	0.160	0.167	0.153	0.168	0.171	0.172	**0.148**	0.152	0.149
	192	0.185	0.199	0.214	0.211	0.182	**0.157**	0.234	0.238	0.263	0.243	0.220	**0.193**	**0.193**	0.196	0.218	0.210	0.212	**0.193**	0.198	0.200	0.205	0.186	0.184	**0.177**
	336	0.244	0.256	0.273	0.261	0.222	**0.206**	0.284	0.283	0.308	0.281	0.256	**0.236**	**0.244**	0.252	0.270	0.259	0.276	0.248	0.231	0.233	0.240	0.214	0.222	**0.212**
	720	0.325	0.333	0.375	0.336	**0.288**	0.290	0.340	0.337	0.388	0.335	0.309	**0.301**	**0.321**	0.330	0.367	0.333	0.380	0.323	0.276	0.276	0.295	0.257	0.277	**0.256**
	Avg	0.224	0.235	0.255	0.241	0.209	**0.193**	0.262	0.263	0.292	0.263	0.242	**0.221**	**0.227**	0.233	0.255	0.241	0.259	0.229	0.218	0.220	0.228	0.201	0.209	**0.199**
ECL	96	0.141	0.144	0.130	0.133	**0.119**	**0.119**	0.247	0.242	0.224	0.220	0.220	**0.212**	**0.130**	0.132	0.131	0.133	0.136	0.133	0.258	0.275	0.167	**0.165**	**0.165**	0.169
	192	0.162	0.165	0.149	0.152	0.136	**0.134**	0.266	0.261	0.241	0.237	0.226	**0.225**	**0.147**	0.151	0.148	0.151	0.153	0.151	0.265	0.282	0.179	0.177	**0.176**	0.181
	336	0.181	0.183	0.172	0.169	0.151	**0.147**	0.284	0.278	0.266	0.255	0.242	**0.239**	**0.164**	0.168	0.169	0.167	0.170	0.167	0.272	0.289	0.197	**0.190**	0.640	0.195
	720	0.219	0.222	0.207	0.207	**0.182**	0.186	0.315	0.309	0.293	0.287	**0.271**	0.274	**0.200**	0.206	0.202	0.205	0.210	0.205	0.287	0.304	0.217	**0.214**	Inf	0.221
	Avg	0.176	0.179	0.165	0.165	**0.147**	**0.147**	0.278	0.272	0.256	0.250	0.240	**0.238**	**0.160**	0.164	0.163	0.164	0.167	0.164	0.270	0.288	0.190	**0.187**	Inf	0.191
Traffic	96	0.382	0.408	0.382	0.380	0.373	**0.350**	0.295	0.283	0.266	0.246	0.245	**0.237**	**0.368**	0.389	0.388	0.392	0.398	0.383	0.335	0.354	0.206	0.193	0.194	**0.190**
	192	0.412	0.434	0.405	0.404	0.399	**0.374**	0.309	0.297	0.274	0.254	0.254	**0.246**	**0.387**	0.410	0.403	0.408	0.415	0.398	0.339	0.359	0.212	0.199	0.199	**0.196**
	336	0.441	0.446	0.421	0.419	0.414	**0.391**	0.326	0.304	0.280	0.261	0.261	**0.253**	**0.411**	0.420	0.414	0.419	0.426	**0.411**	0.345	0.361	0.216	0.204	0.204	**0.201**
	720	0.495	0.508	0.468	0.462	0.460	**0.440**	0.372	0.357	0.307	0.283	0.284	**0.280**	**0.432**	0.450	0.447	0.453	0.465	0.444	0.355	0.376	0.234	0.221	0.222	**0.219**
	Avg	0.433	0.449	0.419	0.416	0.412	**0.389**	0.326	0.310	0.282	0.261	0.261	**0.254**	**0.399**	0.417	0.413	0.418	0.426	0.409	0.343	0.362	0.217	0.204	0.205	**0.202**
Dynamic	60	0.229	0.285	0.234	0.277	0.216	**0.179**	0.214	0.191	0.205	0.183	0.157	**0.109**	**0.240**	0.300	0.246	0.285	0.348	0.250	0.203	0.220	0.165	0.152	0.154	**0.133**
	120	0.302	0.393	0.310	0.363	0.303	**0.275**	0.285	0.271	0.284	0.264	0.227	**0.184**	**0.314**	0.393	0.320	0.367	0.445	0.326	0.241	0.259	0.217	0.208	0.207	**0.187**
	180	0.360	0.465	0.371	0.421	0.350	**0.338**	0.335	0.323	0.337	0.325	0.270	**0.236**	**0.371**	0.460	0.377	0.421	0.521	0.382	0.270	0.289	0.252	0.245	0.243	**0.223**
	300	0.452	0.561	0.455	0.500	0.419	**0.415**	0.409	0.394	0.409	0.398	0.330	**0.301**	0.454	0.554	**0.452**	0.495	0.615	0.456	0.315	0.332	0.296	0.290	0.290	**0.270**
	Avg	0.336	0.426	0.343	0.390	0.322	**0.301**	0.311	0.295	0.309	0.292	0.246	**0.207**	**0.345**	0.426	0.349	0.392	0.482	0.353	0.257	0.275	0.233	0.224	0.224	**0.203**

Table 8: Full Top-3 MSE and Top-3 MAE evaluations of MSE, Mix and MMPD losses across three different backbones on different forecasting horizons τ, which is set to {96, 192, 336, 720} for the first seven datasets and {60, 120, 180, 300} for Dynamic. Bold indicates the best among three losses. Our method is marked in gray.

Metric		Top-3 MSE									Top-3 MAE								
Backbone		Crossformer			SegRNN			MaskAE			Crossformer			SegRNN			MaskAE		
Loss		MSE	Mix	MMPD	MSE	Mix	MMPD	MSE	Mix	MMPD	MSE	Mix	MMPD	MSE	Mix	MMPD	MSE	Mix	MMPD
ETTh1	96	0.365	**0.329**	0.336	0.375	0.354	**0.334**	0.374	0.351	**0.341**	0.406	**0.372**	0.377	0.413	0.389	**0.385**	0.407	0.390	**0.376**
	192	0.417	0.404	**0.369**	0.421	0.466	**0.383**	0.416	0.393	**0.386**	0.437	0.413	**0.398**	0.441	0.448	**0.415**	0.431	0.412	**0.405**
	336	0.462	0.466	**0.399**	0.464	0.423	**0.408**	0.461	0.426	**0.413**	0.464	0.454	**0.420**	0.459	**0.428**	**0.428**	0.458	**0.425**	0.426
	720	0.528	0.533	**0.418**	0.500	0.497	**0.482**	0.503	0.491	**0.457**	0.499	0.492	**0.447**	0.490	**0.464**	0.475	0.492	0.471	**0.455**
	Avg	0.443	0.433	**0.381**	0.440	0.435	**0.402**	0.438	0.415	**0.399**	0.452	0.433	**0.410**	0.451	0.432	**0.426**	0.447	0.425	**0.416**
ETTm1	96	0.274	**0.202**	0.248	0.311	0.254	**0.250**	0.266	0.234	**0.207**	0.340	**0.293**	0.307	0.375	0.332	**0.331**	0.334	0.314	**0.299**
	192	0.347	0.284	**0.269**	0.364	0.313	**0.301**	0.326	0.278	**0.240**	0.384	0.335	**0.333**	0.406	0.366	**0.365**	0.374	0.334	**0.314**
	336	0.399	0.337	**0.328**	0.410	0.347	**0.329**	0.381	0.329	**0.297**	0.410	0.366	**0.365**	0.432	0.391	**0.379**	0.405	0.359	**0.354**
	720	0.492	0.497	**0.395**	0.454	0.428	**0.404**	0.442	0.417	**0.375**	0.455	0.437	**0.407**	0.455	**0.424**	**0.424**	0.443	0.406	**0.401**
	Avg	0.378	0.330	**0.310**	0.385	0.335	**0.321**	0.354	0.314	**0.280**	0.397	0.358	**0.353**	0.417	0.378	**0.375**	0.389	0.353	**0.342**
ETTh2	96	0.301	0.294	**0.250**	0.288	0.275	**0.273**	0.270	0.279	**0.236**	0.359	0.351	**0.326**	0.352	0.341	**0.338**	0.331	0.342	**0.310**
	192	0.368	0.353	**0.304**	0.359	0.356	**0.321**	0.341	0.333	**0.318**	0.402	0.394	**0.363**	0.401	0.399	**0.379**	0.378	0.377	**0.371**
	336	0.386	0.362	**0.327**	0.383	0.355	**0.314**	0.387	0.358	**0.322**	0.420	0.401	**0.377**	0.419	0.397	**0.373**	0.414	0.391	**0.374**
	720	0.433	0.427	**0.377**	0.429	0.380	**0.376**	0.423	0.390	**0.368**	0.468	0.452	**0.422**	0.457	0.419	**0.417**	0.448	0.426	**0.414**
	Avg	0.372	0.359	**0.315**	0.365	0.341	**0.321**	0.355	0.340	**0.311**	0.412	0.400	**0.372**	0.408	0.389	**0.377**	0.392	0.384	**0.367**
ETTm2	96	0.158	0.150	**0.141**	0.173	0.161	**0.142**	0.171	0.191	**0.148**	0.250	0.247	**0.231**	0.267	0.252	**0.239**	0.263	0.250	**0.233**
	192	0.220	0.200	**0.196**	0.236	**0.208**	0.215	0.235	**0.214**	0.223	0.291	0.281	**0.277**	0.314	**0.288**	**0.288**	0.308	**0.285**	**0.285**
	336	0.295	0.255	**0.224**	0.297	0.267	**0.235**	0.306	0.264	**0.261**	0.346	0.321	**0.295**	0.354	0.326	**0.309**	0.358	0.321	**0.311**
	720	0.391	**0.338**	0.350	0.387	0.355	**0.340**	0.409	**0.342**	0.355	0.406	**0.378**	0.379	0.413	**0.378**	0.384	0.420	**0.377**	0.386
	Avg	0.266	0.236	**0.228**	0.273	0.248	**0.233**	0.280	0.253	**0.247**	0.323	0.307	**0.295**	0.337	0.311	**0.305**	0.337	0.308	**0.304**
weather	96	0.134	0.130	**0.120**	0.140	0.140	**0.125**	0.140	0.132	**0.118**	0.189	0.174	**0.157**	0.198	0.179	**0.165**	0.190	0.171	**0.153**
	192	0.186	0.168	**0.164**	0.182	0.189	**0.165**	0.185	0.164	**0.162**	0.241	0.213	**0.202**	0.239	0.234	**0.210**	0.236	0.207	**0.197**
	336	0.247	0.217	**0.210**	0.240	0.233	**0.217**	0.246	0.229	**0.210**	0.296	0.252	**0.241**	0.288	0.266	**0.252**	0.284	0.264	**0.241**
	720	0.327	**0.284**	0.297	0.327	**0.295**	0.296	0.332	**0.287**	0.300	0.347	**0.300**	0.304	0.352	**0.304**	0.309	0.344	**0.309**	**0.309**
	Avg	0.223	0.200	**0.197**	0.222	0.214	**0.201**	0.226	0.203	**0.197**	0.268	0.235	**0.226**	0.269	0.246	**0.234**	0.263	0.238	**0.225**
ECL	96	0.146	0.130	**0.120**	0.145	0.130	**0.122**	0.142	0.122	**0.118**	0.253	0.223	**0.214**	0.252	0.218	**0.217**	0.247	0.213	**0.209**
	192	0.169	0.148	**0.139**	0.168	0.143	**0.136**	0.164	0.139	**0.132**	0.275	0.242	**0.232**	0.273	0.231	**0.229**	0.267	0.230	**0.221**
	336	0.192	0.169	**0.164**	0.188	0.160	**0.151**	0.184	0.156	**0.145**	0.295	0.266	**0.257**	0.292	0.251	**0.244**	0.286	0.245	**0.235**
	720	0.229	0.193	**0.186**	0.230	**0.190**	**0.190**	0.224	0.186	**0.182**	0.327	0.288	**0.279**	0.326	0.280	**0.278**	0.319	0.275	**0.269**
	Avg	0.184	0.160	**0.152**	0.183	0.155	**0.150**	0.178	0.150	**0.144**	0.288	0.255	**0.245**	0.286	0.245	**0.242**	0.280	0.241	**0.234**
Traffic	96	0.397	0.375	**0.367**	0.409	0.388	**0.365**	0.384	0.372	**0.345**	0.310	0.259	**0.248**	0.305	**0.232**	0.242	0.299	0.245	**0.235**
	192	0.436	0.409	**0.389**	0.440	0.419	**0.400**	0.418	0.400	**0.373**	0.326	0.272	**0.253**	0.318	**0.245**	0.251	0.316	0.257	**0.244**
	336	0.453	0.431	**0.405**	0.463	0.432	**0.428**	0.432	0.418	**0.392**	0.341	0.280	**0.260**	0.328	**0.253**	0.263	0.321	0.265	**0.253**
	720	0.518	0.483	**0.456**	0.543	0.516	**0.481**	0.509	0.476	**0.440**	0.391	0.304	**0.283**	0.380	**0.280**	0.285	0.381	0.291	**0.278**
	Avg	0.451	0.424	**0.404**	0.464	0.439	**0.418**	0.436	0.416	**0.387**	0.342	0.279	**0.261**	0.333	**0.253**	0.260	0.329	0.265	**0.253**
Dynamic	60	0.227	0.194	**0.162**	0.228	0.248	**0.176**	0.230	0.205	**0.172**	0.207	0.131	**0.089**	0.212	0.182	**0.108**	0.213	0.149	**0.105**
	120	0.300	0.297	**0.258**	0.304	0.332	**0.266**	0.304	0.301	**0.263**	0.281	0.218	**0.163**	0.285	0.252	**0.185**	0.286	0.224	**0.177**
	180	0.357	0.335	**0.332**	0.356	0.344	**0.328**	0.363	0.342	**0.334**	0.329	0.263	**0.224**	0.329	0.258	**0.239**	0.338	0.267	**0.229**
	300	0.440	**0.401**	0.429	0.445	**0.395**	0.408	0.458	0.437	**0.414**	0.399	0.319	**0.300**	0.403	0.299	**0.308**	0.410	0.338	**0.299**
	Avg	0.331	0.307	**0.295**	0.333	0.330	**0.295**	0.339	0.321	**0.296**	0.304	0.233	**0.194**	0.307	0.247	**0.210**	0.312	0.244	**0.203**

Table 9: Full MSE and CRPS evaluations of MSE, Mix and MMPD losses across three different backbones on different forecasting horizons τ, which is set to {96, 192, 336, 720} for the first seven datasets and {60, 120, 180, 300} for Dynamic. Bold indicates the best among three losses. Our method is marked in gray. Inf indicates the infinity problem caused by outliers.

Metric		MSE									CRPS								
Backbone		Crossformer			SegRNN			MaskAE			Crossformer			SegRNN			MaskAE		
Loss		MSE	Mix	MMPD	MSE	Mix	MMPD	MSE	Mix	MMPD	MSE	Mix	MMPD	MSE	Mix	MMPD	MSE	Mix	MMPD
ETTh1	96	**0.373**	0.418	0.381	0.377	0.396	**0.374**	0.386	0.397	**0.383**	0.320	0.294	**0.293**	0.320	**0.294**	0.296	0.320	**0.293**	0.294
	192	0.419	0.459	**0.403**	**0.419**	0.480	0.424	0.422	0.453	**0.414**	0.337	0.315	**0.305**	0.336	0.330	**0.316**	0.334	0.316	**0.312**
	336	0.455	0.468	**0.422**	**0.454**	**0.454**	0.460	0.454	0.464	**0.428**	0.349	0.332	**0.324**	0.346	Inf	**0.331**	0.347	**0.320**	0.328
	720	0.512	0.495	**0.456**	0.484	0.480	**0.479**	0.487	0.508	**0.457**	0.370	0.352	**0.335**	**0.363**	Inf	0.369	0.363	0.345	**0.340**
	Avg	0.440	0.460	**0.416**	**0.433**	0.452	0.434	0.437	0.456	**0.421**	0.344	0.323	**0.314**	0.341	Inf	**0.328**	0.341	**0.319**	**0.319**
ETTm1	96	**0.293**	0.309	0.345	0.324	**0.317**	0.332	**0.294**	0.323	0.298	0.284	**0.244**	0.266	0.297	**0.261**	0.273	0.282	0.258	**0.255**
	192	0.360	**0.351**	0.355	0.368	**0.359**	0.389	0.333	0.339	**0.316**	0.307	**0.260**	0.272	0.315	Inf	**0.292**	0.300	0.262	**0.259**
	336	0.398	**0.378**	0.409	0.401	0.390	**0.380**	0.375	0.373	**0.350**	0.323	**0.280**	0.295	0.328	Inf	**0.301**	0.317	**0.278**	0.285
	720	0.478	0.559	**0.445**	**0.439**	0.460	0.445	0.428	0.448	**0.405**	0.351	0.340	**0.316**	0.346	**0.321**	0.328	0.339	0.312	**0.310**
	Avg	**0.382**	0.399	0.388	0.383	**0.381**	0.386	0.357	0.371	**0.342**	0.316	**0.281**	0.287	0.321	Inf	**0.299**	0.310	**0.277**	**0.277**
ETTh2	96	0.332	**0.326**	0.329	**0.312**	0.320	0.319	**0.288**	0.338	0.296	0.285	**0.286**	0.288	0.278	**0.275**	0.281	**0.260**	0.281	0.265
	192	0.399	0.394	**0.376**	0.379	0.388	**0.373**	**0.364**	0.394	0.372	0.316	0.320	**0.311**	0.313	**0.312**	0.314	**0.296**	0.310	0.306
	336	0.393	0.421	**0.373**	0.389	**0.374**	0.384	0.393	0.408	**0.371**	0.324	0.330	**0.319**	0.321	Inf	**0.317**	**0.317**	0.320	0.318
	720	0.428	0.472	**0.419**	0.425	**0.417**	0.430	0.418	0.435	**0.408**	0.351	0.356	**0.346**	0.345	**0.329**	0.340	0.338	Inf	**0.331**
	Avg	0.388	0.403	**0.374**	0.376	**0.375**	0.376	0.366	0.394	**0.362**	0.319	0.323	**0.316**	0.314	Inf	**0.313**	**0.303**	Inf	0.305
ETTm2	96	**0.166**	0.177	0.174	0.185	0.182	**0.173**	0.184	**0.182**	**0.182**	0.197	0.200	**0.195**	0.211	**0.197**	0.206	0.207	**0.196**	0.200
	192	0.234	**0.226**	0.241	0.247	**0.241**	0.265	**0.248**	0.257	0.256	0.228	**0.225**	0.231	**0.243**	Inf	0.244	0.239	**0.231**	0.244
	336	0.299	0.297	**0.272**	**0.300**	0.324	0.307	0.310	0.319	**0.303**	0.264	0.260	**0.251**	0.270	0.303	**0.261**	0.273	**0.262**	0.270
	720	**0.387**	0.391	0.391	**0.383**	0.391	0.397	0.405	0.406	**0.382**	0.309	**0.308**	0.318	**0.313**	Inf	0.317	0.318	**0.309**	0.318
	Avg	0.271	0.273	**0.270**	**0.279**	0.285	0.285	0.287	0.291	**0.281**	0.249	**0.248**	0.249	0.259	Inf	**0.257**	0.259	**0.250**	0.258
WTH	96	**0.144**	0.156	0.148	0.151	0.170	**0.149**	**0.149**	0.162	0.150	0.166	**0.147**	0.150	0.172	Inf	**0.156**	0.168	0.148	**0.147**
	192	**0.196**	0.209	0.199	**0.188**	0.249	0.191	0.194	0.211	**0.192**	0.202	0.186	**0.185**	0.198	0.211	**0.192**	0.199	Inf	**0.181**
	336	**0.250**	0.263	0.253	**0.241**	0.305	0.248	**0.247**	0.330	0.248	0.238	0.219	**0.217**	0.232	0.240	**0.227**	0.233	0.251	**0.216**
	720	**0.322**	0.336	0.326	**0.323**	0.368	0.340	**0.328**	0.377	0.333	0.279	**0.255**	0.263	0.281	Inf	**0.267**	0.279	0.276	**0.261**
	Avg	**0.228**	0.241	0.232	**0.226**	0.273	0.232	**0.230**	0.270	0.231	0.221	**0.202**	0.204	0.221	Inf	**0.210**	0.220	Inf	**0.201**
ECL	96	0.138	0.147	**0.133**	**0.134**	0.152	0.135	**0.130**	0.137	**0.130**	0.261	Inf	**0.170**	0.260	Inf	**0.170**	0.258	**0.166**	**0.166**
	192	0.156	0.168	**0.154**	0.155	0.171	**0.154**	0.149	0.156	**0.147**	0.268	Inf	**0.186**	0.267	Inf	**0.183**	0.265	0.179	**0.178**
	336	**0.176**	0.193	0.187	**0.171**	0.194	0.172	0.166	0.173	**0.164**	0.276	Inf	**0.209**	0.275	Inf	**0.196**	0.273	0.192	**0.191**
	720	0.210	0.222	**0.208**	0.210	0.231	**0.206**	0.204	0.214	**0.202**	0.291	Inf	**0.224**	0.291	Inf	**0.222**	0.289	0.238	**0.216**
	Avg	**0.170**	0.182	**0.170**	0.168	0.187	**0.167**	0.162	0.170	**0.161**	0.274	Inf	**0.197**	0.273	Inf	**0.193**	0.271	0.194	**0.188**
Traffic	96	**0.386**	0.427	0.398	0.390	0.425	**0.383**	**0.371**	0.408	0.375	0.339	0.205	**0.198**	0.337	Inf	**0.192**	0.335	0.195	**0.189**
	192	0.412	0.443	**0.409**	0.412	0.446	**0.409**	0.395	0.427	**0.394**	0.344	0.211	**0.202**	0.341	Inf	**0.199**	0.341	0.203	**0.195**
	336	0.422	0.460	**0.419**	0.431	0.463	**0.429**	**0.402**	0.442	0.406	0.348	0.216	**0.207**	0.344	Inf	**0.207**	0.342	0.207	**0.201**
	720	**0.454**	0.507	**0.454**	0.477	0.536	**0.464**	0.446	0.488	**0.440**	0.362	0.234	**0.223**	0.358	Inf	**0.222**	0.358	0.226	**0.218**
	Avg	**0.418**	0.459	0.420	0.428	0.468	**0.421**	**0.403**	0.441	0.404	0.348	0.217	**0.208**	0.345	Inf	**0.205**	0.344	0.208	**0.201**
Dynamic	60	0.238	0.326	**0.237**	**0.238**	0.367	**0.238**	**0.241**	0.335	0.245	0.201	Inf	**0.119**	0.202	0.172	**0.130**	0.204	0.149	**0.132**
	120	0.311	0.432	**0.308**	0.313	0.454	**0.311**	**0.316**	0.441	**0.316**	0.237	Inf	**0.171**	0.239	Inf	**0.187**	0.242	0.204	**0.183**
	180	**0.366**	0.493	0.380	0.369	0.474	**0.368**	**0.376**	0.511	0.379	0.266	Inf	**0.215**	0.268	Inf	**0.225**	0.273	0.241	**0.222**
	300	**0.441**	0.570	0.472	**0.446**	0.565	**0.446**	0.462	0.615	**0.458**	0.307	Inf	**0.271**	0.310	Inf	**0.274**	0.317	0.293	**0.270**
	Avg	**0.339**	0.455	0.349	0.342	0.465	**0.341**	**0.349**	0.476	0.350	0.253	Inf	**0.194**	0.255	Inf	**0.204**	0.259	0.222	**0.202**

F Additional Experiments on Hyper-Parameters

Table 10: Metrics comparison of different noise schedules on ETTh1 ($T = 336, \tau = 96$). The default schedule used in main experiments is marked in gray.

	Top-3 MSE	Top-3 MAE	MSE	CRPS
Quadratic	**0.314**	**0.362**	0.379	**0.286**
Cosine	0.317	0.364	0.382	0.289
Linear	0.329	0.371	**0.375**	0.289

Table 11: Top-3 MSE/MAE evaluations versus varying maximum number of modes M in Algorithm 1 on ETTh1 ($T = 336, \tau = 96$). The default setting in main experiments is marked in gray.

M	5	10	15	20	25
Top-3 MSE	0.3200	0.3197	0.3200	0.3199	0.3203
Top-3 MAE	0.3667	0.3667	0.3668	0.3667	0.3668

Table 12: Top-3 MSE/MAE evaluations versus varying mixture weights prior hyperparameter ρ in Algorithm 1 on ETTh1 ($T = 336, \tau = 96$).

ρ	0.1	0.3	0.5	0.7	0.9
Top-3 MSE	0.329	0.322	0.320	0.314	0.307
Top-3 MAE	0.377	0.378	0.367	0.358	0.354

Table 13: Top-3 MSE/MAE evaluations versus varying variance prior hyperparameter u in Algorithm 1 on ETTh1 ($T = 336, \tau = 96$).

u	0.001	0.01	0.1	1	10	100	1000
Top-3 MSE	0.322	0.321	0.323	0.323	0.318	0.320	0.314
Top-3 MAE	0.372	0.371	0.372	0.372	0.361	0.367	0.364

Noise Schedule. In our main experiments, we use the linear schedule as default. Table 10 further evaluates two advanced schedules: Quadratic (Kong & Ping, 2021) and Cosine (Nichol & Dhariwal, 2021). Results show that MMPD benefits from these advanced schedules. This indicates that developing time-series-specific schedules is a promising direction, since time series and image data have fundamentally different characteristics.

Diffusion Steps in Training. Fig. 7 demonstrates that increasing the number of training diffusion steps K_{train} significantly improves Top-3 MSE, Top-3 MAE and MSE. Notably, this enhancement comes without computational overhead during inference, as we employ resampling with fixed inference steps K_{infer}. For our experiments, we adopt $K_{train} = 1,000$ as the default setting.

Diffusion Steps in Inference. Fig. 8 shows that increasing the number of inference diffusion steps K_{infer} consistently improves prediction accuracy. However, as revealed by our efficiency analysis in Table 4, this improvement comes with increased computational overhead. To achieve a balance between accuracy and efficiency, we set $K_{infer} = 20$ as our default configuration.

Anchor step k^* in Eq. 8. Fig. 9 shows that overly large $\bar{\alpha}_{k^*}$ harms multi-mode and probabilistic prediction, while small ones degrade deterministic prediction. The performance is robust across a broad range around $\bar{\alpha}_{k^*} = 0.5$. To maintain a simple formulation of Eq. 8, we choose k^* to make $\bar{\alpha}_{k^*}$ close to 0.5.

Maximum number of modes M in Algorithm 1. Table 11 shows that the multi-mode accuracy remains robust w.r.t M. This arises from using a variational GMM rather than a standard one. In this formulation, only the maximum number of modes needs to be specified, while the inference algorithm automatically determines the appropriate number of active modes. This behavior is illustrated in Fig. 3(c), where we set $M = 10$, but only 3 modes are activated after inference.

Mixture weights prior hyperparameter ρ in Algorithm 1. ρ controls the prior over the number of activated modes-a larger ρ encourages utilizing more modes. Table 12 shows that larger ρ leads to slightly lower Top-3 MSE/MAE, but activating too many modes may confuse downstream users.

Variance prior hyperparameter u in Algorithm 1. u influences the prior over the variance, where a larger value reflects greater confidence in the variance estimated from forward diffusion. As shown in the Table 13 below, performance remains robust.

G Detailed FLOPs Analysis

FLOPs of MSE Loss. MSE loss uses a conventional MLP to project latent tokens into future series. A conventional S-block MLP consists of three components:

- One linear input layer with $O(d^2)$ FLOPs;

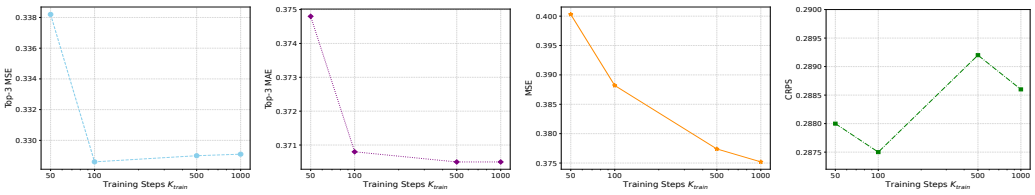

(a) (b) (c) (d)

Figure 7: (a) Top-3 MSE, (b) Top-3 MAE, (c) MSE, (d) CRPS evaluations versus varying diffusion steps in training (K_{train}) on ETTh1 ($T = 336, \tau = 96$). The Linear noise schedule is used and the diffusion steps in inference are set to $K_{infer} = 20$.

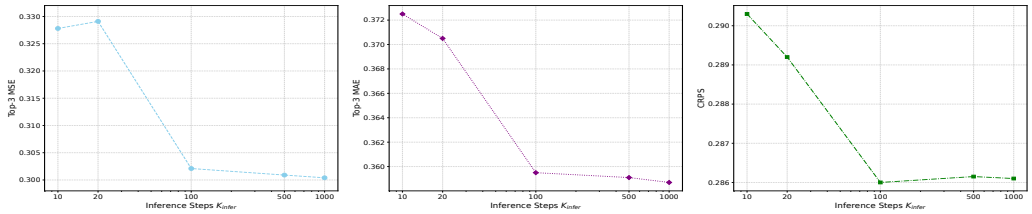

(a) (b) (c)

Figure 8: (a) Top-3 MSE, (b) Top-3 MAE, (c) CRPS evaluations versus varying diffusion steps in inference (K_{infer}). $K_{train} = 1,000$ and other settings are same as Fig. 7. MSE is omitted as K_{infer} does not affect deterministic prediction.

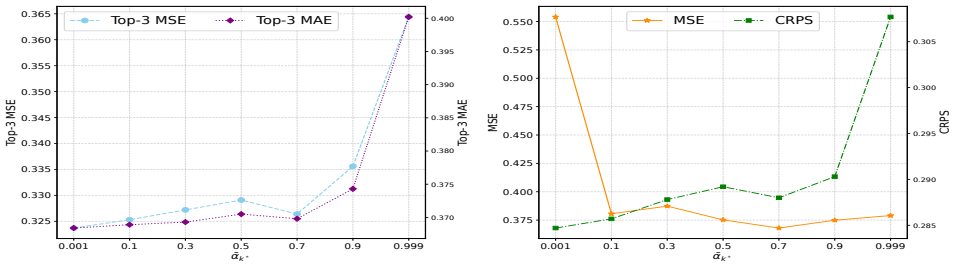

(a) (b)

Figure 9: (a) Top-3 MSE & Top-3 MAE, (b) MSE & CRPS evaluations versus varying $\bar{\alpha}_{k^*}$ in Eq. 8 on ETTh1 ($T = 336, \tau = 96$).

- S hidden blocks, each has two linear layers and one activation layer between them. The FLOPs are $O(2d^2)$;
- One linear output layer with $O(Pd)$ FLOPs;

Therefore, the FLOPs for a conventional MLP applied to one token is $O\left((2S+1)d^2 + Pd\right)$. To predict a series of length τ, this MLP is simultaneously applied to τ/P tokens, making the total FLOPs $F_{MLP} = O(\frac{\tau}{P}[(2S+1)d^2 + Pd])$.

For both training and deterministic inference, MSE loss requires one backbone forward pass and one MLP forward pass, so the FLOPs are $F_{bkb} + F_{MLP}$. It should be noted that MSE loss cannot perform probabilistic or multi-mode prediction, marked with "N/A" in Tables 4.

FLOPs of MMPD Loss. MMPD loss uses Patch Consistent MLP as the denoising network, which is slightly more complex than the conventional MLP above. A S-block Patch Consistent MLP consists of three components:

- Input operations in Eq. 7, requiring $O(d^2 + (2r+1)Pd)$ FLOPs;
- S AdaLN-MLP blocks in Eq. 12, each requires $O(5d^2)$ FLOPs;
- One AdaLN output block in Eq. 13, requiring $O(2d^2 + Pd)$ FLOPs;

Same as MSE, the Patch Consistent MLP is simultaneously applied to τ/P tokens, so the total FLOPs are $F_{PC-MLP} = O(\frac{\tau}{P}[(5S+3)d^2 + (2r+2)Pd])$.

As for EM steps in Algorithm 1, three vector operations contribute most FLOPs and other scalar operations are negligible. The three vector operations are: 1) Computation of $\ln \gamma_{nm}^k$ requires $O(3\tau MN)$; 2) $\boldsymbol{\mu}_m^k$ requires $O(2\tau MN)$; 3) $\widetilde{v}_m^k$ requires $O(3\tau MN)$. So one EM step has the FLOPs of $F_{EM} = O(8\tau MN)$.

For training, MMPD Loss requires one backbone forward pass and two Patch Consistent MLP passes: one for the diffusion objective and another for the deterministic objective in Eq. 8. So the training FLOPs are $F_{bkb} + 2F_{PC-MLP}$. Considering the backbone dominates training cost (i.e., $F_{bkb} >> F_{MLP}, F_{PC-MLP}$), training FLOPs of MMPD remain nearly identical to those of MSE.

Similar to MSE, deterministic inference of MMPD loss requires one backbone forward pass and one Patch Consistent MLP forward pass, so the FLOPs are $F_{bkb} + F_{PC-MLP}$, differences only lie in MLP architectures. For probabilistic and multi-mode predictions, MMPD needs to generate N samples, each through K diffusion-EM iterations. So the FLOPs are $F_{bkb} + K(NF_{PC-MLP} + F_{EM})$. As $F_{EM} << NF_{PC-MLP}$, we omit it in Table 4 for simplicity. To generate one instance, MMPD loss only requires a single backbone pass, followed by K lightweight MLP passes, making its cost significantly lower than that of TS Diffusion models requiring K backbone passes.

H Further Discussion: Extending MMPD to Non-patch-based Backbones

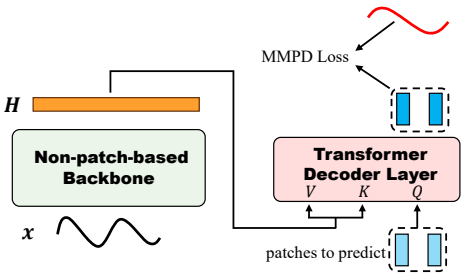

Figure 10: Adapting non-patch-based backbones to use MMPD loss: a single Transformer decoder layer is inserted between the backbone and MMPD. In this layer, backbone output $\mathbf{H}$ serves as key and value, while learnable tokens indicating patches to predict act as the queries. The decoder output is then used for MMPD loss computation.

The latent representations $\mathbf{H}$ extracted by non-patch-based backbones are not naturally expressed as $\{\mathbf{h}_j\}_{j=1}^l$, thus MMPD loss cannot be directly applied. As illustrated in Fig. 10, we address this by inserting a single Transformer decoder layer: $\mathbf{H}$ serves as key and value, while learnable tokens indicating prediction patches act as query. This decoder layer transforms $\mathbf{H}$ into tokens suitable for MMPD loss.

Using this adaptation, we apply MMPD to following non-patch-based backbones: **1) TSMixer** (Chen et al., 2023), a fully MLP model without patching; **2) iTransformer** (Li et al., 2024b), a non-patch-based Transformer designed to model inter-channel dependencies. Table 14 shows that our adaptation with MMPD loss performs on par with the original architectures using MSE loss in deterministic forecasting, while significantly outperforming them in multi-mode and probabilistic forecasting. This demonstrates the effectiveness of our adaptation and highlights the potential of applying MMPD to a broader range of backbones.

Table 14: Comparison of non-patch-based backbones (TSMixer and iTransformer) trained using MSE loss and adapted MMPD loss on datasets ETTh1/ETTm1/WTH, $T = 336, \tau = 192$.

Dataset		ETTh1	ETTm1	WTH	ETTh1	ETTm1	WTH	ETTh1	ETTm1	WTH	ETTh1	ETTm1	WTH
Metric		Top-3 MSE			Top-3 MAE			MSE			CRPS		
TSMixer	MSE	0.384	0.285	0.140	0.415	0.353	0.198	0.390	0.306	0.149	0.323	0.289	0.169
	MMPD	**0.367**	**0.230**	**0.118**	**0.396**	**0.309**	**0.161**	**0.378**	0.306	**0.148**	**0.304**	**0.260**	**0.150**
iTransformer	MSE	0.390	0.298	0.147	0.414	0.361	0.200	0.400	**0.317**	**0.158**	0.324	0.292	0.173
	MMPD	**0.361**	**0.279**	**0.132**	**0.395**	**0.326**	**0.180**	**0.386**	0.334	0.170	**0.304**	**0.278**	**0.165**

I Further Discussion: Extending MMPD to Multi-task Learning

Beyond the traditional single-dataset paradigm, we further extend the MMPD loss to multi-task learning, where a unified model is trained across multiple datasets and settings. Such a model can directly perform multi-task forecasting and be adapted to few-shot or zero-shot forecasting on new datasets.

Table 15: Multi-task forecasting comparison of UNITS pretrained with MSE and MMPD loss on 20 forecasting tasks.

Metric	MSE		MAE		Top-3 MSE		Top-3 MAE		CRPS	
Pretraining Loss	MSE	MMPD	MSE	MMPD	MSE	MMPD	MSE	MMPD	MSE	MMPD
NN5	0.618	**0.595**	0.551	**0.530**	0.623	**0.572**	0.559	**0.512**	0.453	**0.390**
ECL-96	0.168	**0.161**	0.270	**0.260**	0.178	**0.146**	0.285	**0.241**	0.271	**0.189**
EC-192	0.184	**0.175**	0.283	**0.272**	0.195	**0.163**	0.301	**0.256**	0.280	**0.201**
ECL-336	0.203	**0.192**	0.300	**0.289**	0.203	**0.174**	0.313	**0.270**	0.285	**0.211**
ECL-720	0.242	**0.229**	0.331	**0.318**	0.234	**0.215**	0.338	**0.302**	0.300	**0.234**
ETTh1-96	0.397	**0.367**	0.420	**0.400**	0.377	**0.325**	0.413	**0.367**	0.334	**0.286**
ETTh1-192	0.438	**0.408**	0.448	**0.427**	0.433	**0.386**	0.443	**0.404**	0.353	**0.312**
ETTh1-336	0.465	**0.442**	0.465	**0.448**	0.456	**0.436**	0.458	**0.425**	0.365	**0.325**
ETTh1-720	0.507	**0.472**	0.500	**0.478**	0.513	**0.474**	0.496	**0.464**	0.394	**0.347**
Exchange-192	0.261	**0.225**	0.364	**0.343**	0.223	**0.160**	0.338	**0.279**	0.318	**0.274**
Exchange-336	0.464	**0.415**	0.494	**0.469**	0.349	**0.306**	0.429	**0.393**	0.439	**0.372**
ILI	**2.073**	2.345	**0.895**	0.967	2.045	**1.981**	0.894	**0.855**	**0.739**	0.785
Traffic-96	0.475	**0.446**	0.314	**0.288**	0.483	**0.414**	0.343	**0.265**	0.352	**0.211**
Traffic-192	0.484	**0.460**	0.314	**0.292**	0.477	**0.426**	0.336	**0.268**	0.350	**0.211**
Traffic-336	0.498	**0.477**	0.319	**0.299**	0.519	**0.465**	0.349	**0.280**	0.357	**0.219**
Traffic-720	0.532	**0.510**	0.336	**0.315**	0.545	**0.507**	0.359	**0.299**	0.361	**0.233**
Weather-96	**0.163**	0.166	0.214	**0.213**	0.149	**0.136**	0.203	**0.173**	0.176	**0.166**
Weather-192	**0.212**	0.213	0.257	**0.254**	**0.178**	0.180	0.236	**0.220**	0.212	**0.202**
Weather-336	**0.267**	0.270	0.297	**0.294**	0.269	**0.245**	0.268	**0.267**	0.251	**0.241**
Weather-720	**0.344**	0.353	0.347	**0.345**	**0.323**	0.328	**0.317**	0.327	0.300	**0.287**
Winning Counts	5/20	**15/20**	1/20	**19/20**	2/20	**18/20**	1/20	**19/20**	1/20	**19/20**

Table 16: Few-shot forecasting comparison of UNITS tuned with MSE and MMPD loss on new datasets. For each setting, only 5% of the training set is used for prompt-based tuning.

Metric	MSE		MAE		Top-3 MSE		Top-3 MAE		CRPS	
Prompt Tuning Loss	MSE	MMPD	MSE	MMPD	MSE	MMPD	MSE	MMPD	MSE	MMPD
ETTh2-96	0.409	**0.377**	0.415	**0.403**	0.382	**0.341**	0.409	**0.374**	0.326	**0.292**
ETTh2-192	**0.380**	0.381	**0.398**	0.403	0.365	**0.335**	0.389	**0.373**	0.343	**0.318**
ETTh2-336	**0.436**	0.447	**0.437**	0.445	0.415	**0.397**	0.431	**0.413**	0.361	**0.347**
ETTh2-720	0.449	**0.445**	0.454	**0.453**	0.431	**0.420**	0.458	**0.447**	0.382	**0.361**
SaugeenRiverFlow	1.270	**1.248**	0.576	**0.569**	1.128	**1.088**	0.510	**0.485**	0.543	**0.480**
Winning Counts	2/5	**3/5**	2/5	**3/5**	0/5	**5/5**	0/5	**5/5**	0/5	**5/5**

We evaluate this idea using UNITS (Gao et al., 2024), a unified multi-task model that integrates multiple tasks within a single framework. Since our focus is solely on forecasting, we adopt the supervised variant (UNITS-SUP) without incorporating classification techniques. As a patch-based model originally trained and tuned with MSE loss, MMPD loss can be integrated into it with minimal changes to enhance its ability to capture complex distributions.

Multi-task Forecasting. Following Gao et al. (2024), we first conduct multi-task supervised pretraining on 20 forecasting tasks using either MSE or MMPD loss. Results in Table 15 show that for deterministic forecasting measured by MSE/MAE, MMPD loss matches or improves performance over MSE. A possible reason is that MMPD provides a more challenging objective that encourages richer representations, which are especially beneficial in multi-task scenarios. For multi-mode and probabilistic forecasting measured by Top-3 MSE/MAE and CRPS, UNITS trained with MMPD significantly outperforms its MSE-trained counterpart. This demonstrates that MMPD integrates well with UNITS and effectively enables the modeling of complex distributions.

Few-shot Forecasting. We then tune the pretrained models with MSE and MMPD loss to perform few-shot prediction on new datasets. In each setting, only 5% of the training data is utilized and the prompt-based tuning from Gao et al. (2024) is used. As shown in Table 16, MMPD matches MSE in deterministic accuracy while consistently outperforming it in probabilistic and multi-mode forecasting.

Zero-shot Forecasting. Finally, Table 17 evaluates zero-shot forecasting capabilities of models pretrained with MSE and MMPD. Results are consistent with the few-shot setting: MMPD maintains comparable deterministic accuracy while offering superior probabilistic and multi-mode performance.

Table 17: Zero-shot forecasting comparison on new datasets of pretrained UNITS using MSE and MMPD.

Metric	MSE		MAE		Top-3 MSE		Top-3 MAE		CRPS	
Pretraining Loss	MSE	MMPD	MSE	MMPD	MSE	MMPD	MSE	MMPD	MSE	MMPD
Solar	0.202	**0.169**	0.320	**0.299**	0.207	**0.095**	0.331	**0.193**	0.272	**0.187**
River	2.336	**2.294**	**0.735**	0.746	2.298	**1.722**	0.733	**0.722**	0.643	**0.624**
Hospital	**1.115**	1.175	**0.818**	0.834	0.998	**0.860**	0.772	**0.705**	0.690	**0.622**
Winning Counts	1/3	**2/3**	**2/3**	1/3	0/3	**3/3**	0/3	**3/3**	0/3	**3/3**

J VISUALIZATIONS

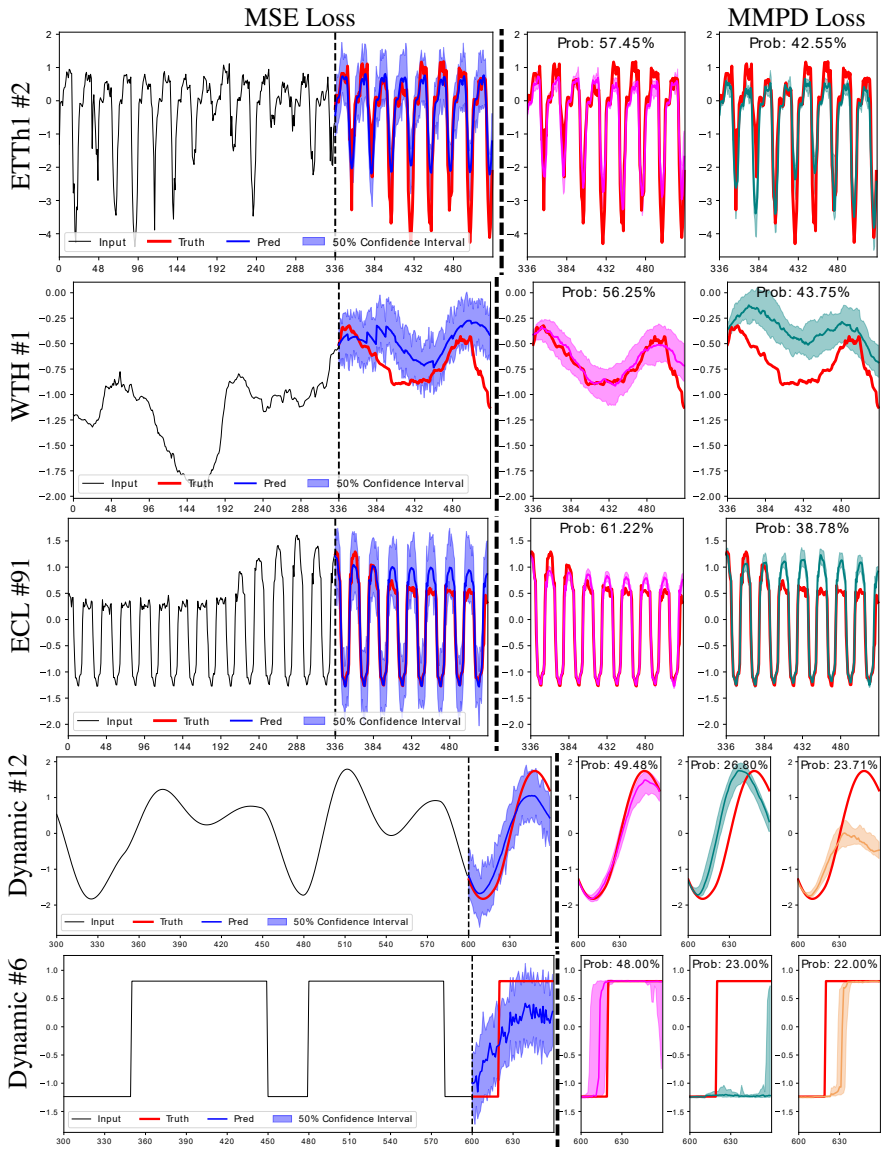

Figure 11: Forecasting cases of MSE loss *vs.* MMPD loss. Each row represents one instance, with the dataset name and channel number indicated on the left. Predictions from MSE and MMPD losses are separated by a thick vertical dashed line. On the left, one-mode predictions generated by the MSE loss are shown, along with the corresponding input series. On the right, multi-mode predictions generated by the MMPD loss are displayed, with their corresponding probabilities shown at the top.

K DECLARATION OF LARGE LANGUAGE MODELS USAGE

In this work, large language models were used solely for word choice and language polishing. They did not contribute to research ideation, methodology or analysis.